Journal of Inorganic Biochemistry 219 (2021) 111437

Contents lists available at ScienceDirect

Journal of Inorganic Biochemistry

journal homepage: www.elsevier.com/locate/jinorgbio

Control of distal lysine coordination in a monomeric hemoglobin: A role for heme peripheral interactions

Jaime E. Martinez Grundman [a], Laia Julió Plana [b], Jamie L. Schlessman [c], Luciana Capece [b,*], Darío A. Estrin [b], Juliette T.J. Lecomte [a,**]

[a] T.C. Jenkins Department of Biophysics, Johns Hopkins University, Baltimore, MD 21218, USA
[b] Departamento de Química Inorgánica, Analítica y Química Física, Facultad de Ciencias Exactas y Naturales, Universidad de Buenos Aires, Instituto de Química Física de los Materiales, Medio Ambiente y Energía (INQUIMAE)-CONICET, C1428EGA Buenos Aires, Argentina
[c] Chemistry Department, U.S. Naval Academy, Annapolis, MD 21402, USA

ARTICLE INFO

Keywords:
Truncated hemoglobin
Hexacoordinate hemoglobin
Distal ligand
Heme redox potential
Lysine ionization
pH/redox coupling

ABSTRACT

THB1 is a monomeric truncated hemoglobin (TrHb) found in the cytoplasm of the green alga *Chlamydomonas reinhardtii*. The canonical heme coordination scheme in hemoglobins is a proximal histidine ligand and an open distal site. In THB1, the latter site is occupied by Lys53, which is likely to facilitate Fe(II)/Fe(III) redox cycling but hinders dioxygen binding, two features inherent to the NO dioxygenase activity of the protein. TrHb surveys show that a lysine at a position aligning with Lys53 is an insufficient determinant of coordination, and in this study, we sought to identify factors controlling lysine affinity for the heme iron. We solved the "Lys-off" X-ray structure of THB1, represented by the cyanide adduct of the Fe(III) protein, and hypothesized that interactions that differ between the known "Lys-on" structure and the Lys-off structure participate in the control of Lys53 affinity for the heme iron. We applied an experimental approach (site-directed mutagenesis, heme modification, pH titrations in the Fe(III) and Fe(II) states) and a computational approach (MD simulations in the Fe(II) state) to assess the role of heme propionate–protein interactions, distal helix capping, and the composition of the distal pocket. All THB1 modifications resulted in a weakening of lysine affinity and affected the coupling between Lys53 proton binding and heme redox potential. The results supported the importance of specific heme peripheral interactions for the pH stability of iron coordination and the ability of the protein to undergo redox reactions.

1. Introduction

The binding of ligands to hemoglobin (Hb) and myoglobin (Mb) has been the subject of multiple kinetic, thermodynamic, and structural studies ([1] and references therein). Two canonical states are typically invoked in the association reaction with O_2: a five-coordinate (5c) heme with the proximal histidine as the sole axial ligand to the ferrous iron (Fig. 1B) and a six-coordinate (6c) heme with O_2 bound on the distal side (Fig. 1A). In the superfamily of hemoglobins, however, several functional proteins provide two axial residues to the heme, making a third state (endogenous 6c, Fig. 1C) necessary to describe ligand binding reactions [2]. How specific features of the polypeptide contribute to the differential stabilization of various states and therefore the reactivity of the heme is a question that knowledge of amino acid sequence or homology modeling cannot yet answer. Here we take an experimental and computational approach to explore the structural underpinnings of

Abbreviations: 4c, four-coordinate; 5c, five-coordinate; 6c, six-coordinate; BIS-TRIS, bis-(2-hydroxy-ethyl)-amino-tris(hydroxymethyl)-methane; DME, dimethyl ester; DME-heme, Fe(II)-protoporphyrin IX dimethyl ester; DME-hemin, Fe(III)-protoporphyrin IX dimethyl ester; DME-Mb, myoglobin containing DME-heme or DME-hemin; DME-THB1, THB1 containing DME-heme or DME-hemin; DT, sodium dithionite; EE THB1, K49E/R52E THB1; FII THB1, Y29F/Q50I/Q54I THB1; GlbN-A, GlbN with covalently attached heme (vinyl-His117); Hb, hemoglobin; HP, high-pressure; LT, long tunnel; Mb, myoglobin; MD, molecular dynamics; MP8, microperoxidase 8; NP4, nitrophorin 4; NPT, isothermal-isobaric; PDB, Protein Data Bank; RMSD, root-mean-squared deviation; SVD, singular-value decomposition; TrHb, truncated hemoglobin; TrHb1, group 1 truncated hemoglobin; Tris, tris(hydroxymethyl)aminomethane; WT, wild-type.

* Corresponding author at: Dto. de Química Inorgánica, Analítica y Química Física - INQUIMAE-CONICET, Fac. de Ciencias Exactas y Naturales, Univ. de Buenos Aires, Cdad. Universitaria, CABA C1428EGA, Argentina.
** Co-Correspondence to: T.C. Jenkins Department of Biophysics, Johns Hopkins University, 3400 North Charles Street, Baltimore, MD 21218, USA.
E-mail addresses: lula@qi.fcen.uba.ar (L. Capece), lecomte_jtj@jhu.edu (J.T.J. Lecomte).

https://doi.org/10.1016/j.jinorgbio.2021.111437
Received 13 October 2020; Received in revised form 20 March 2021; Accepted 20 March 2021
Available online 24 March 2021

distal site ligation in THB1, an endogenous 6c hemoglobin from *Chlamydomonas reinhardtii*.

THB1 is a monomeric "group 1 truncated hemoglobin" (TrHb1) residing in the cytosol [3,4]. Initial studies demonstrated that cellular levels of THB1 depend on the availability of nitrate and thus established a link between THB1 and nitrogen metabolism [5], likely involving NO dioxygenase activity. Subsequent studies reinforced the relationship of THB1 to NO management [6–8] and supported THB1's role in the nitrogen cycle of *C. reinhardtii* [9]. The heme axial ligands in this protein are a histidine (His77) at the proximal site and a neutral lysine (Lys53) at the distal site [5]. Binding of O_2, as necessary for aerobic function, therefore requires the decoordination of Lys53, and THB1 exhibits each of the equilibria depicted in Fig. 1. The role of THB1 as an NO dioxygenase also requires the protein to cycle between Fe(II) and Fe(III) states. Lysine, as a ligand common to Fe(II) and Fe(III) THB1, has been proposed to accelerate the step restoring the Fe(II) state after nitrate release [10]. The redox potential of the iron couple, besides affecting electron transfer rates [11], has significance for its connection to the relative stability of the Fe(III) and Fe(II) states [12]. In THB1 and heme proteins in general, it is a well-controlled characteristic related to holoprotein integrity and reactivity [13,14].

Three practical features make THB1 well suited for a thermodynamic analysis of the factors controlling the differential stabilization of possible holoprotein states: 1) the acid lability of lysine coordination; 2) the accessibility of the two oxidation states visited during NO dioxygenation; and 3) the spectroscopic signatures associated with different ligation schemes and oxidation states. Acidification converts the endogenous 6c THB1 to a 5c complex (His–—Fe) when in the Fe(II) state or a water-bound complex (exogenous 6c, His–Fe–OH_2) when in the Fe (III) state. The acid decoordination of Lys53, coupled to protonation of the amino headgroup and protein structural changes, has an apparent pK_a of ~6.5 in either the Fe(III) or Fe(II) oxidation state [5]. Compared to the pK_a value of a solvent-exposed lysine (10.4 [15]) an apparent pK_a of 6.5 reflects the large energetic cost (~22 kJ/mol) expended by the folded protein to maintain the lysine in the neutral state. As a consequence, measurements of apparent pK_a values in modified THB1s in Fe (II) and Fe(III) oxidation states report on the effect of the modifications on the energetics of proton binding, lysine coordination, and redox potential.

The X-ray structure of Fe(III) THB1 with coordinated lysine is available to 1.9 Å resolution (PDB ID 4XDI [16]) and is valid for the Fe (II) state in solution [5]. This crystal structure (Fig. 2) offers clues for the stabilization of THB1 in the Lys-coordinated or "Lys-on" state. In particular, two basic residues on the E helix, Lys49 (E6) and Arg52 (E9), interact directly with the heme propionates and block entrance to the heme distal side [16]. The N-capping Asp46 (E3) is also at the heme periphery and is a potential control point for E helix stability and Lys53 coordination. Similarly, the well-conserved set of polar residues at positions B10/E7/E11 (Tyr29, Gln50, and Gln54 in THB1) is expected to contribute to the energetic balance through participation in buried H-bonds with (or without) an exogenous ligand.

We hypothesize that the interactions described above control the coordination of Lys53. The detection of structural differences involving the implicated residues in the "Lys-off" state would constitute a first level of support. We therefore solved the X-ray structure of Fe(III) THB1 with bound cyanide to represent the "Lys-off" state and confirmed the plausibility of our hypotheses. As a second level of testing, we disrupted the interactions with amino acid replacements or a heme modification, and analyzed the pH response of these altered proteins in the Fe(II) and Fe(III) oxidation states. Throughout the manuscript, the apparent pK_a refers to the pH midpoint of the transition connecting the Lys-on state and the Lys-off state. Complementary molecular dynamics (MD) simulations were carried out to provide structural and dynamic insights that are inaccessible experimentally. The results are consistent with our hypothesis concerning heme–protein interactions; in addition they provide energetic assessments and suggest ways in which distal ligation and the conformational state of the protein can be controlled by pH.

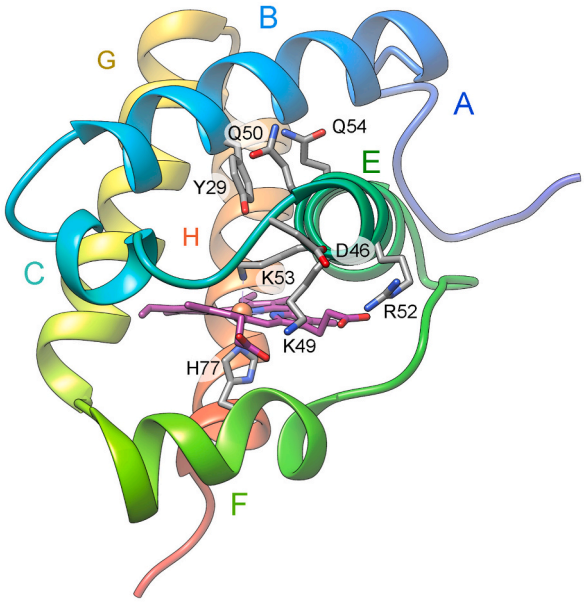

Fig. 2. The crystal structure of THB1 in the Lys-on state (PDB ID 4XDI chain A [16]). The heme group and Tyr29 (B10), Asp46 (E3), Lys49 (E6), Gln50 (E7), Arg52 (E9), Lys53 (E10), Gln54 (E11), and His77 (F8) are represented with sticks. The helices are labeled A, B, C and E, F, G, H as per the canonical Mb notation.

2. Material and methods

2.1. Experimental methods

2.1.1. Protein preparation and purification

The codon-optimized sequence of *C. reinhardtii* THB1 (UniProt ID A8JAR4) cloned into a pJExpress414 plasmid (ATUM, Newark, CA) was used for all recombinant work. The THB1 variants K49E, R52E, K49E/

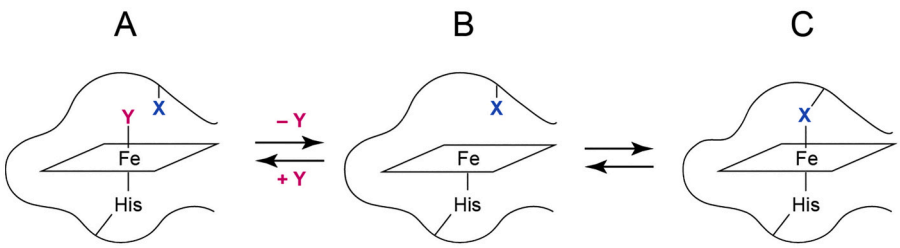

Fig. 1. Schematic diagram of states encountered in hemoglobins: "His" represents the proximal histidine; the porphyrin ring is a parallelogram; X is a residue (distal histidine in sperm whale Mb or distal lysine in THB1); and Y is a small exogenous ligand, for example O_2 for Fe(II) and H_2O or CN^- for Fe(III). A: represents the exogenous 6c state; B: the 5c state; and C: the endogenous 6c state.

R52E (EE for short), D46L, and Y29F/Q50I/Q54I (FII for short) were obtained by polymerase chain reaction mutagenesis using PfuTurbo (Agilent) or Q5 High-Fidelity (NEB) DNA polymerase and custom primers (Integrated DNA Technologies, Inc., Coralville, IA). Sequences were verified by GENEWIZ, Inc. (South Plainfield, NJ). Overexpression and purification steps were carried out as previously reported [5] to yield pure apoprotein. Heme reconstitution followed a published protocol [5] except in the case of D46L THB1, which developed a side product with a broad blue shoulder to the Soret band. This species was eliminated by adding dissolved hemin directly to urea-solubilized protein and allowing slow refolding via extensive dialysis in Tris-EDTA buffer prior to chromatography steps. The purity of preparations was verified using sodium dodecyl sulfate polyacrylamide gel electrophoresis, and holoproteins were exchanged into 5 mM potassium phosphate buffer at pH 7.0, lyophilized, and stored at −20 °C. Mass spectrometry analysis (Acquity/Xevo-G2, Waters) returned molecular masses consistent with initial methionine cleavage and the desired amino acid replacements. Protein concentrations for the THB1 variants were calculated using extinction coefficients determined using hemochromogen assays [17,18] and reference spectra in potassium phosphate buffer.

Reconstitution of wild-type (WT) THB1 with Fe(III) protoporphyrin IX dimethyl ester (DME-hemin, Frontier Scientific, Logan, UT) followed the warm methanol method published for Fe(III) DME-Mb [19]. The purified Fe(III) DME-THB1 had a A_{406}/A_{277} ratio ~3.2 at pH 7.0. Compared to WT THB1 (A_{409}/A_{280} ~5.6 at pH 7.0), the ratio indicated ~60% reconstitution. This holoprotein yield was sufficient to obtain useful electronic absorption data while avoiding damage caused by a prolonged reconstitution process.

The state of the DME cofactor after reconstitution was verified by thin-layer chromatography. A cofactor sample, rapidly extracted from Fe(III) DME-THB1 at pH 2 with cold butanone, was spotted on a silica plate, alongside standard samples of Fe(III) DME-hemin dissolved in acidified butanone and hemin chloride dissolved in alkaline butanone. A 20:1 2,6-lutidine:H_2O solvent mixture was used as the mobile phase [20]. The R_f values determined for DME-hemin (0.98), hemin chloride (0.02), and extracted DME-hemin from Fe(III) DME-THB1 (0.90–0.98) confirmed the integrity of the ester moieties.

2.1.2. X-ray structure determination

A 20 mg/mL solution of Fe(III) THB1 was incubated with 3.5-fold excess potassium cyanide for several hours, then combined in a 3 μL:1 μL ratio with reservoir solution consisting of 0.1 M bis-(2-hydroxyethyl)-amino-tris(hydroxymethyl)-methane (BIS-TRIS), pH 5.5 and 30% *w/v* polyethylene glycol 3350. Within approximately two weeks, crystals of cyanomet THB1 were obtained at room temperature via hanging drop vapor diffusion. A diffraction data set was collected to 1.70 Å resolution from a single crystal (coated in Paratone oil as a cryoprotectant) using CuKα radiation on a Rigaku Oxford Diffraction Supernova diffractometer, processed and scaled using CrysalisPro software (Agilent).

Experimental single-wavelength anomalous diffraction phasing was carried out using PHENIX AutoSol [21], including heavy atom (Fe) identification, density modification, and automated model building. This was followed by rounds of manual model building in Coot [22] and automatic refinement using PHENIX Refine. Model quality in the final stages was assessed using MolProbity [23]. Molecular graphics and analysis (such as root-mean-square deviation (RMSD) calculations, helix crossing parameters, etc.) were performed with UCSF Chimera [24]. Internal cavities and tunnels were identified using MOLEonline v.2.5 [25].

2.1.3. pH titrations monitored by electronic absorption spectroscopy

All pH measurements were carried out with a Mettler Toledo microsensor combined pH electrode calibrated with pH 4.00, 7.00, and 10.00 standard pH buffers (Fisher Scientific). For pH titrations in the Fe (III) state, a sample was prepared from lyophilized protein in 5 mM potassium phosphate buffer at pH ~7. The sample was divided into two cuvettes, and the pH of each was adjusted incrementally by addition of stock solutions (0.1–1 M) of HCl or NaOH. For titrations under high salt concentration (0.5 M KCl), the difference in liquid junction potential between the standard buffers and sample was expected to cause inaccurate measurements [26]. To correct for this error, the pH meter calibrations were performed with ionic-strength-corrected buffers prepared by addition of KCl to the standard pH buffers [27] and using KOH as the alkaline titrant. Electronic absorption spectra were collected from 250 to 750 nm, acquired in 0.5-nm steps with 0.25-s averaging time in a Cary50 UV–Vis spectrophotometer (Agilent Technologies) at room temperature.

For pH titrations of proteins in the Fe(II) state, separate samples of ~10–15 μM protein were prepared in 100 mM buffer solutions ranging from pH 5.5 to 11. Sodium citrate was used for pH 5.0–5.4, 2-(N-morpholino)ethanesulfonic acid for pH 5.7–6.4, 3-(N-morpholino)propanesulfonic acid for pH 6.5–7.5, Tris for pH 7.7–8.4, borate for pH 8.7–9.8, and N-cyclohexyl-3-aminopropanesulfonic acid for 10.1–11.1. Spectra were collected prior to reduction to determine heme concentrations based on the known pH response of each variant. Minor spectral differences were corrected for by scaling with absorbance values at the isosbestic points of the Fe(III) pH titration. The samples were reduced with addition of sodium dithionite (DT) to 2 mM and monitored over time with spectra collected from 350 to 650 nm, in 1-nm steps with 0.1-s averaging time at room temperature. Once the absorbance remained constant, the spectrum was selected for inclusion in the titration analysis. Data from some of the variants showed evidence of a low-pH 4c–5c transition. Such data were excluded from the fitting. We note that the measurements in the Fe(II) states do carry a higher uncertainty than the measurements in the Fe(III) state.

Singular-value decomposition (SVD) was performed using Mathematica 12 (Wolfram) or MatLab R2019a (MathWorks) on each spectral data matrix $A(\lambda_m,pH_n)$ to yield $A = U(\lambda)\cdot S\cdot V(pH)^T$ [28]. In each case, the S matrix indicated how many V vectors were sufficient to reproduce the data. For all variants in the selected pH ranges, two V vectors were significant and used for global fitting with a single-site proton binding equation according to.

$$V_k(pH) = \frac{a_k \times 10^{n\left(pK_{a,i}-pH\right)} + b_k}{10^{n\left(pK_{a,i}-pH\right)} + 1} \quad (1)$$

where a_k and b_k are the values of the k vector at low pH and high pH, respectively, and n (Hill coefficient) and $K_{a,i}$ (apparent ionization or ligand switching constant in redox state $i = 2$ or 3) are common to both vectors. Pure component spectra were reconstructed as the matrix $D(\lambda_m, pH_n)$ using the curtailed $U_{m,2}$ and $S_{2,2}$ matrices, along with the fitted parameter matrix $H = \begin{pmatrix} b_1 & a_1 \\ b_2 & a_2 \end{pmatrix}$ according to $D = U_{m,2}(\lambda)^T\cdot S_{2,2}\cdot H$. Values are reported with error of the fit.

Under low pH conditions (pH << 10.4) and when there is no ligand replacing the axial lysine (6c ⇆ 5c process), $pK_{a,i} = pK_i + pK_{out,K}$, where $K_{out,K}$ represents the acid dissociation constant of the lysine, once exposed to solvent ($pK_{out,K} = 10.4$), and K_i is an apparent constant that captures both lysine affinity for the heme iron and the energetics of conformational change. This is the case for Fe(II) proteins and the FII variant. When there is competition between lysine and a water molecule for the ferric iron (overall endogenous 6c ⇆ exogenous 6c process), the apparent constant reflects relative affinities and conformational energetics, $pK_{a,i} = pK_i - pK_{OH2} + pK_{out,K}$. In this expression, K_{OH2} represents the "association" constant for a molecule of H_2O binding to the 5c state corrected for water concentration, i.e., [THB1-OH_2]/[THB1, 5c]. H_2O/Lys exchange is associated with $pK_{ex} = pK_i - pK_{OH2}$. Finally, if the affinity of water for the iron is low, the fraction of 5c protein must be included as an additional term. Derivations relating the apparent pK_a and ligand affinities for iron are included in the Supplementary Material.

2.1.4. NMR data collection

Samples of Fe(III) K49E, R52E, EE, D46L, and FII variants were prepared in 20 mM or 100 mM phosphate buffer, pH ~7, and 10% ^2H_2O. One-dimensional ^1H spectra were acquired on a Bruker Avance-600 or Bruker Avance II-600 at 25 °C with at least a 100 kHz spectral width to capture the hyperfine-shifted signals appearing near ~80 ppm. The cyanomet complexes were generated with at least 5-fold KCN added to each sample and equilibrated for at least 1 h before data collection. For these spectra, a width of 32–34 kHz was sufficient. All data were analyzed with TopSpin 4.0.6 (Bruker BioSpin).

High-pressure (HP) NMR characterization of two test variants, K49E and R52E, was carried out to assess their pressure response at pH conditions close to the calculated pK_a values. Lyophilized proteins were solubilized in degassed baroresistant buffer mixtures [29]: 15 mM Tris, 5 mM phosphate, pH 8.0 for K49E, and 14.1 mM Tris, 5.9 mM phosphate, pH 7.5 for R52E. Each sample was layered with mineral oil in a zirconia HP-NMR tube and pressurized with an Xtreme-60 pump (Daedalus Innovations), using degassed water as the transducing fluid. At each 250-bar pressure step up to 2500 bar, samples were equilibrated at 25 °C for 5 min. All spectral changes associated with increasing pressure were fully reversible.

2.2. Molecular dynamics simulations

Classical molecular dynamics simulations were performed to complement the experimental data. As a control, two Lys-off simulations were performed with the cyanomet WT THB1 structure (PDB ID 6CII, this work): one in the Fe(III) state in a 6c complex with cyanide and His77 as axial ligands, and another in the Fe(II) state in a 5c complex with cyanide deleted and His77 as the sole ligand. These simulations served to gauge the dynamic stability of this conformation of THB1 as a general Lys-off structural model. For all THB1 variants (K49E, R52E, EE, D46L and FII), the MD simulations were performed starting with the conformation observed in the Lys-on structure (PDB ID 4XDI [16]) but with the iron in the Fe(II) state and after releasing the Fe-Lys53 bond constraint. In these Fe(II) 5c simulations, the decoordinated Lys53 was set as either neutral or protonated inside the heme cavity. Simulations in the 6c Lys-on state were not performed as we were primarily concerned with the fate of the lysine once the Fe–Nζ bond was broken. Protonation states of amino acid residues were set to correspond to those at physiological pH. In the case of histidine residues, protonation states were established in order to favor H-bond formation as in previous works [30–33], with the exception of the proximal His77, which was protonated at the Nδ1 atom.

All MD simulations were performed using the PMEMD module of the Amber16 package [34], in its graphical process unit version. The starting structures were immersed in an octahedral box of three-site transferrable intermolecular potential water molecules [35] and a minimum distance of 15 Å from the protein surface to the end of the box was used. Residue parameters correspond to AMBER ff14SB force field [36] except for the heme. The parameters of the 5c heme correspond to those developed [37] and used in several heme–protein studies [30,38–43]. Parameters for the cyanide bound Fe(III) heme were taken from reference [44]. All simulations were performed using periodic boundary conditions with a 10 Å cutoff and particle mesh Ewald summation method for treating the electrostatic interactions. The SHAKE algorithm was employed to keep bonds involving hydrogen atoms at their equilibrium lengths [45], which allowed a 2-fs time step for the integration of Newton's equations. All simulations were performed in the isobaric-isothermal (NPT) ensemble, at 1 atm and 300 K using the Berendsen barostat [46] and the Langevin thermostat [47]. Equilibration consisted of an energy minimization of the initial structures, followed by a slow heating up to the chosen temperature, with a temperature ramp of 0.375 K per ps. All production MD simulations were run for 300 ns.

Analysis of the MD simulations was performed using Visual Molecular Dynamics (VMD) [48], UCSF Chimera [24], and the Cpptraj tool from Amber16 package [34].

3. Results

3.1. The structure of cyanomet THB1

THB1 in the Fe(III) Lys-off state has a molecule of water bound on the distal side [5,10]. This aquomet complex is detected at low pH, but under those conditions, its limited solubility and propensity for heme loss prevent the preparation of samples suitable for structural analysis. In contrast, cyanide is a high-affinity ligand [49] expected to remain bound to Fe(III) over a broad range of pH and in the presence of various additives. Cyanide and water are both small and capable of forming hydrogen bonds. Moreover, the aquomet structure of *Paramecium caudatum* TrHb1, which possesses Lys E10, forms the same set of interactions as detected in the cyanide bound (cyanomet) complex of *C. eugametos* TrHb1 [50]. Therefore, in this work we used cyanomet THB1 as a structural surrogate for the aquomet state of THB1.

3.1.1. Main features

Cyanomet THB1 crystallizes in the $P4_122$ space group with a single protein molecule in the asymmetric unit. Phasing was achieved with single-wavelength anomalous diffraction from the heme iron, and the resulting model was refined to 1.70 Å resolution. All but four N-terminal and seven C-terminal residues located outside the globin domain were well defined. Electron density maps of the heme group, the proximal histidine, cyanide ligand, and residues near bound cyanide are shown in Fig. 3. The average heme plane is perpendicular to the proximal imidazole plane, and out-of-plane heme distortions (mostly ruffling and saddling) [51] appear moderate at this resolution. Data collection information and refinement statistics are given in the experimental section and in Table 1. Coordination geometries for the cyanomet structure are listed in Table S1 along with the corresponding information for the Lys-on structure for comparison.

All seven α-helices characteristic of the TrHb1 fold appear clearly in the structure. These elements of secondary structure are labeled A–C and E–H in Fig. 4A. In addition, a turn of 3_{10} helix is formed before the A helix proper. Several helix capping interactions are conserved features of TrHb1s [17,52,53] and are found in cyanomet THB1 as well. For example, the side chain of the highly conserved Asp35 forms a hydrogen bond with Gln37 NH, providing an N-cap to the C helix. A similar N-cap is seen for the E helix, formed by Asp46 and the backbone NH of both Lys48 and Lys49, and for the F helix, formed by Asp72 and Ala75 NH. The G helix is N-terminated with a hydrogen bond between His90 Nδ1 and Asn87 NH. Table 2 lists these and other selected polar or ionic interactions present in THB1 (a full list is provided in Table S2).

The residues surrounding the heme are depicted in Fig. 4B. On the proximal side, the environment is dominated by hydrophobic side chains. On the distal side, Gln50 (E7), Gln54 (E11), along with Tyr29 (B10) and cyanide (Fig. 3B), form the distal network of hydrogen bonds typical of TrHb1s [50]. Opposed to Gln50 and Gln54, residues Phe28 (B9), Phe42 (CD1), and Ile32 (B13) provide a hydrophobic wall protecting Tyr29 (B10). These interactions are consistent with those observed in the majority of TrHb1s when an exogenous ligand is bound.

TrHb1s that coordinate the heme with two residues (His/His or His/Lys) have a compact structure with no obvious path for small ligands to access the heme group [16,17,54,55]. However, in the His/Y state (where Y is an exogenous ligand, Fig. 1A), tunnels within the protein matrix are observed in all TrHb1s. These tunnels connect the distal side to solvent [54,55] and presumably facilitate the diffusion of diatomic ligands such as O_2 and NO to the reactive iron center [56]. Cyanomet THB1 displays such network of tunnels (Fig. S4). The main branch known as the long tunnel (LT) originates between the GH turn and the first turn of the B helix, extending toward to E helix. It is noteworthy that Met58 (E15) is found in two rotameric states shaping the LT in alternative ways. This situation is reminiscent of the dual orientation of Phe

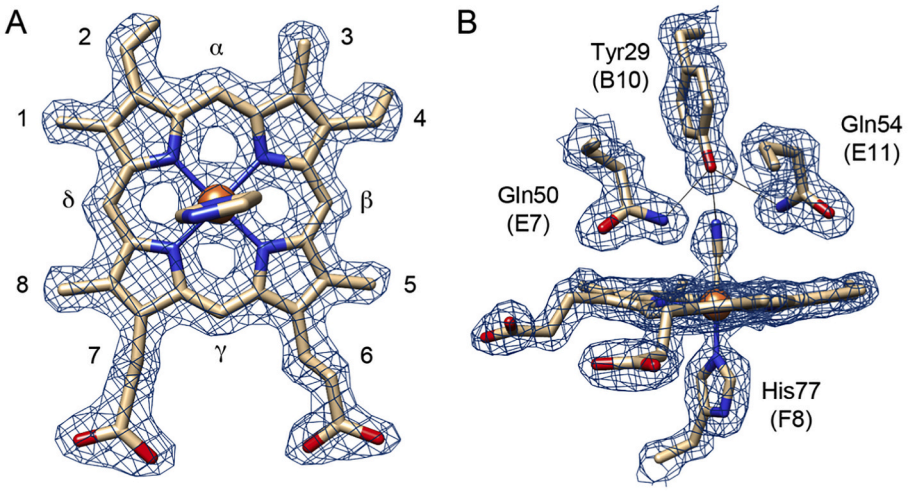

Fig. 3. $2F_o - F_c$ electron density maps contoured at the 1.0 σ level. A: The heme group viewed from the proximal side including peripheral heme substituents labeled as used in the text. B: The heme group viewed from the edge with cyanide ligand and distal pocket residues forming the hydrogen bonding network.

Table 1
Data collection and refinement statistics for the crystal structure of cyanomet THB1.

Crystal data and collection statistics	
Space group	$P\,4_1\,2\,2$
Unit cell *a*, *b*, *c* (Å)	45.99, 45.99, 121.28
Unit cell *α*, *β*, *γ* (°)	90.00, 90.00, 90.00
Wavelength (Å)	1.54
Resolution (Å)	21.50–1.70 (1.76–1.70)
No. of reflections (total/unique)	224,603/27,344 (13,529/2,732)
Completeness (%)	99.9 (99.9)
R-merge (%)	4.2 (19.2)
Redundancy	8.2 (5.0)
Mean $I/\sigma(I)$	36.06 (5.88)
Wilson *B* factor (Å^2)	15.0
Refinement statistics	
Resolution range (Å)	21.50–1.70 (1.73–1.70)
Data cutoff ($\sigma(F)$)	1.35
No. of reflections (work/test)	24,622 (1,287)/ 2,722 (142)
R-work/R-free (%)	16.3/19.1 (19.2/26.8)
CC-work/CC-free (%)	96.4/95.7 (92.2/86.8)
RMSD bonds (Å)	0.010
RMSD angles (°)	1.40
Number of atoms	1190
Protein	1005
Ligands	45
Solvent	140
Average B-factor (Å^2)	18.2
Protein	17.2
Ligands	14.3
Solvent	27.8
Ramachandran favored (%)	100.0

Values in parentheses are for the highest resolution shell.

E15 in *Mycobacterium tuberculosis* HbN [57,58]. A second tunnel (referred to as EH) has an exit between the beginning of the EF loop and a C-terminal distortion of the H helix and connects with the LT to establish a continuous network of conserved cavities. Thus, cyanomet THB1 appears as porous as other TrHb1s and offers the same access paths to the iron, including through the E15 gate [56].

3.1.2. Comparison with the Lys-on structure

To gauge the conformational flexibility of THB1 and identify differential interactions related to lysine (de)coordination, we compared the Lys-on (PDB ID 4XDI) and Lys-off (cyanomet, PDB ID 6CII) states. Superimposition of the two structures (Fig. 5A) returns a minimized Cα RMSD of 2.3 Å across all 124 possible pairs (Table S3, Fig. S1). The C, F,

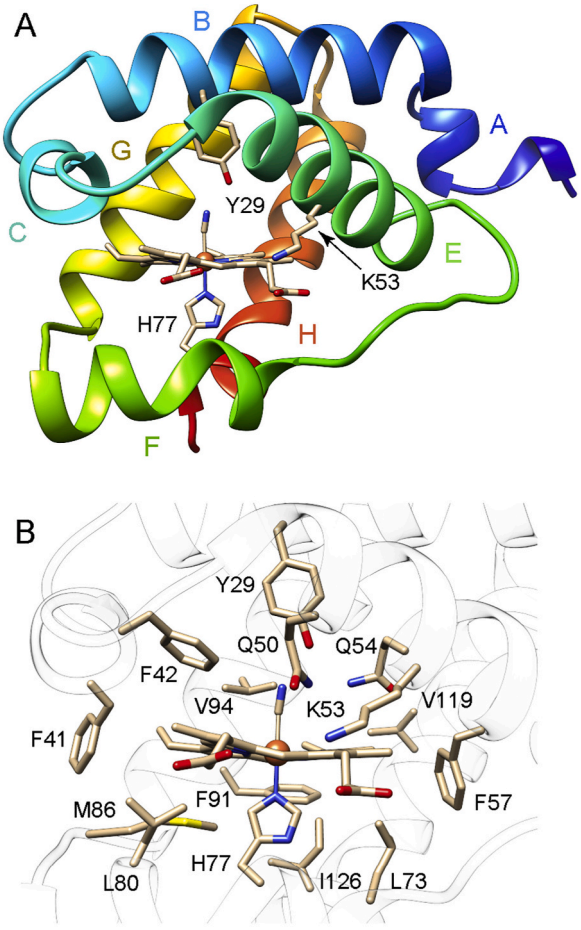

Fig. 4. A: Ribbon diagram of cyanomet THB1 (PDB ID 6CII). Helical elements were identified using DSSP [97] as implemented in UCSF Chimera [24] and are labeled according to the Mb notation: A (11–14), B (17–33), C (39–42), E (47–61), F (73–83), G (88–104), and H (109–127). Note that the Mb numbering is out of step with the TrHb secondary structure, for example, residue E4 is the first residue of the THB1 E helix. B: Stick diagrams of selected residues surrounding the heme cofactor and cyanide molecule.

Table 2
Select side chain polar and ionic interactions in Fe(III) THB1 crystal structures.

Interacting residues	Description	His–Fe–Lys (4XDI)	His–Fe–CN^- (6CII)
Tyr29, Gln50, Gln54, CN^-	Distal H-bonds		✓
Asp35, Gln37 NH	C helix N-cap	✓	✓
Asp46, Lys48/Lys49 NH	E helix N-cap	✓	✓
Lys49, 6-propionate	Protein-heme	✓	
Arg52, 7-propionate	Protein-heme	✓	
Lys53, 7-propionate	Protein-heme		✓
Asp72, Ala75 NH	F helix N-cap	✓	✓
His90, Asn87 NH	G helix N-cap	✓	✓

G, and H helices overlap with minimized pairwise distances generally lower than 0.5 Å. Relative to these elements of structure, significant displacements are observed for the A, B, and E helices. In particular, the E helix rotates about its long axis expelling the distal Lys53 to solvent and reorienting against the rest of the fold. To characterize this topological feature rigorously, we calculated helix crossing parameters [59] in each structure (Fig. 5B and Fig. S2). The polar plot illustrates that the rearrangement of the B/E helix crossing in THB1 is similar to the rearrangement exhibited by other pairs of TrHb1s [60], although differences are detected in the "ridges into grooves" packing of the Lys-on conformation compared to other endogenous 6c TrHb1s (Fig. S3).

Fig. 6 compares the distal heme pocket and heme periphery of the two THB1 structures in detail. The ionic contacts noticed in the Lys-on structure between Lys49 (E6) and the heme 6-propionate, and between Arg52 (E9) and the heme 7-propionate are disrupted in the cyanomet structure following the rotation of the E helix, while Lys53 (E10) directs its now protonated Nζ amino group to the heme 7-propionate. In a concerted fashion, residues Tyr29 (B10), Gln50 (E7), and Gln54 (E11) rearrange to participate in the buried H-bonding network described above. The Asp46 N-cap, which is partially formed in chain B of the Lys-on structure, is fully populated in the cyanomet structure.

3.2. Structural models of other THB1 states

At this time, the structure of the 5c state of THB1 is not available. Other globins must therefore be used as guides to infer conformational properties. The mini-hemoglobin from *Cerebratulus lacteus* in the "deoxy" state (PDB ID 4AVE) [61] offers a close match. This protein exhibits no conformational change between the aquomet state and the deoxy state. Residues Tyr B10, Gln E7, and Thr E11 maintain a distal hydrogen bond network, while Lys E10 forms an ionic interaction with a heme propionate. Likewise in Fe(II) THB1, it is conceivable that once Lys53 (E10) is decoordinated, its protonated side chain reaches out to the solvent and the conformation switches to that of the cyanomet structure, stabilized by the B10/E7/E11 interactions inside the distal pocket. Thus, in what follows, structure 4XDI is used to represent the endogenous 6c (His/Lys) state whereas all 5c and exogenous 6c states are taken to be similar to the cyanomet structure solved here (PDB ID 6CII).

3.3. Choice of THB1 modifications

To probe lysine coordination in THB1, we used a heme modification and amino acid replacements. To test the role of the heme carboxylates, we reconstituted WT apoTHB1 with Fe(III) protoporphyrin IX dimethyl ester (DME-hemin). We also made single and double replacements of Lys49 (E6) and Arg52 (E9) with Glu residues (K49E, R52E, and K49E/R52E) to reverse charges while avoiding large changes in helical propensity. The involvement of the E helix in the Lys-on/Lys-off transition and prior results identifying the beginning of the E helix as a dynamic element of structure in TrHb1s [62] prompted an investigation of the E helix N-cap with the D46L replacement. In addition, the composition of the distal heme pocket was modified by the Y29F/Q50I/Q54I (FII) triple

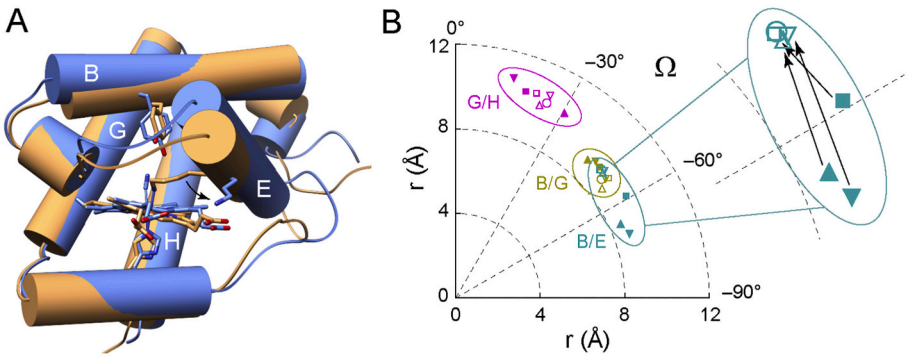

Fig. 5. Differences in interhelical arrangement upon ligand switching in THB1. A: Superimposed structures of Lys-on THB1 (PDB ID 4XDI, orange) and Lys-off/cyanomet THB1 (blue). Note the position of the distal Lys53, the tilt in the heme plane, and the rearrangement of the A, B, and E helices upon cyanide ligand binding. B: Polar plot of calculated helix crossing parameters [59] for the helix pairs B/E (dark cyan), B/G (dark yellow), and G/H (magenta) as defined by DSSP in UCSF Chimera [24]. The arrows in the magnified plot of B/E crossings indicate endogenous 6c → exogenous 6c ligand switching. The data are for *C. eugametos* cyanomet TrHb1 (PDB ID 1DLY, open circles), *Synechocystis* sp. PCC 6803 GlbN-A in the *bis*-His state (PDB ID 1RTX, closed up-triangles) and the cyanomet state (PDB ID 1S69, open up-triangles), *Synechococcus* sp. PCC 7002 GlbN-A in the *bis*-His state (PDB ID 4MAX, closed down-triangles) and the cyanomet state (PDB ID 4L2M, open down-triangles), and THB1 in the Lys-on state (closed squares) and the cyanomet state (open squares). (For interpretation of the references to colour in this figure legend, the reader is referred to the web version of this article.)

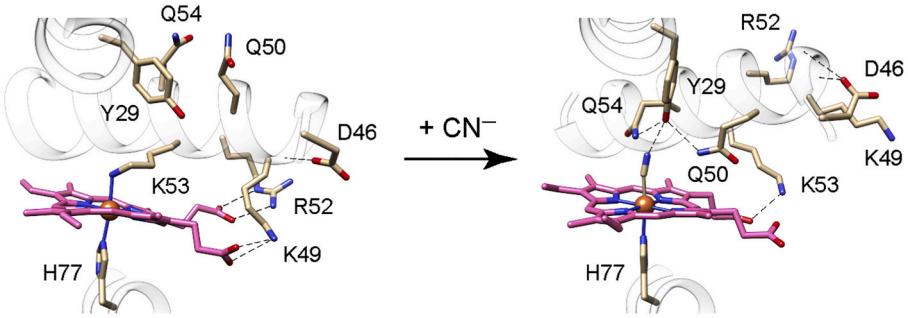

Fig. 6. Selected residues in the periphery of the heme cofactor in THB1, highlighting changes upon distal Lys53 decoordination and exogenous ligand (cyanide) binding. Residues Tyr29 (B10), Gln50 (E7), and Gln54 (E10) form the distal H-bonding network conserved in TrHb1s, while Lys53 is relocated to the protein exterior within H-bonding distance to the heme 6-propionate. Both Arg52 (E9) and Lys49 (E6) are also displaced from their heme propionate interactions with the conformational change, while the Asp46 N-cap remains intact. The residues in the figure, except His77 and Lys53, were modified in this work.

Table 3
Optical properties of various THB1s in selected states.

Protein	pH	Soret (nm)	Q (nm)	CT[a] (nm)	ε at Soret max[b] (mM^{-1} cm^{-1})
Fe(III)					
WT[c]	4.8	408	503, 542 (sh)	630	144
	10.8	412	538, 570 (sh)		118
DME	5.7	403	502, 536 (sh)	630	ND
	10.9	408	537, 566 (sh)		
D46L	6.0	406	503, 538 (sh)	632	133
	11.0	411	539, 567 (sh)		119
K49E	5.6	407	501, 539 (sh)	632	149
	11.1	411	540, 565 (sh)		114
R52E	5.6	406	501, 539 (sh)	630	151
	11.1	411	539, 566 (sh)		114
K49E/R52E	5.6	405	501, 539 (sh)	631	158
	11.1	411	538, 566 (sh)		117
Y29F/Q50I/Q54I	5.3	404	506, 540 (sh)	639	ND
	10.0	411	539, 564 (sh)		
Fe(II)					
WT	10.03	426	529	559	195
DME	11.03	423	527	559	ND
D46L	11.05	426	529	560	217
K49E	11.10	425	528	559	207
R52E	11.12	425	528	559	210
K49E/R52E	11.08	426	529	559	212
Y29F/Q50I/Q54I	10.07	425	529	560	ND

[a] Charge transfer band.
[b] Determined by the hemochromogen assay at a single pH and scaled using the titration data; ND, not determined.
[c] From [5].

replacement, meant to disrupt the distal hydrogen bonding network and to create a highly hydrophobic environment at the distal site.

3.4. Preliminary characterization of modified Fe(III) THB1s

At pH values < 6, the Glu variants, E helix N-cap variant and DME-THB1 display high-spin electronic absorption spectra resembling the WT aquomet (His–Fe–OH_2) complex (Table 3). In contrast, FII THB1 has a low intensity and blue-shifted Soret band. According to its coordinate in the plot of Soret ε vs Soret λ_{max} devised by Shikama [63], the Fe(III) heme of FII THB1 does not bind a water molecule. This observation parallels those reported for the Y(B10)F/Q(E11)V and Y(B10)L/Q(E11)V variants of *M. tuberculosis* HbN [64], in which the removal of H-bonding residues at B10 and E11 led to the stabilization of a 5c species. Hydrophobic distal cavities are known to promote the 5c state also in full-length globins [63,65]. In the context of our study, the population of an Fe(III) 5c state makes FII THB1 a unique protein with which to inspect the energetics of Lys53 coordination in the absence of water competition.

At pH > 10, all proteins showed 6c low-spin features, expected to be due to the formation of His–Fe–Lys complexes. This assumption needed to be validated because a bound water molecule can readily be ionized, yielding a hydroxymet state (His–Fe–OH^-) with a low-spin spectrum resembling that of a His–Fe–Lys state. We therefore compared the high pH spectra (or components of the spectral decomposition, see Section 2.1.3) of a series of THB1 variants. The visible region of five of these is shown in Fig. 7. The spectra of WT, K49E, and EE THB1 (shown) and FII, R52E and D46L THB1 (not shown for clarity) are superimposable, whereas those of K53R THB1 [66] and K53A THB1 [5], neither of which can adopt a His–Fe–Lys state but do form hydroxymet complexes under the chosen conditions, are clearly different. Thus, we conclude that the Lys-on state is the first state reached when the pH of each inspected aquomet or 5c protein is raised.

To verify the properties of the Lys-off state, we collected the ^{1}H 1D NMR spectra of the 6c variants at neutral pH. High-spin aquomet spectra are obtained (Fig. S5) with some chemical shift variations but no hint of extensive rearrangement compared to aquomet K53A THB1 [5]. Interestingly, the EE variant spectrum resembles the spectrum of R52E THB1, which suggests a stronger influence of this residue on the electronic structure of the heme group in the high-spin state. In addition to the heme aquomet signals, the R52E and D46L variants show some low-spin (His–Fe–Lys) signals (e.g., ~24 ppm), whereas K49E and EE show very little if any such contribution at the same pH. Thus, in EE THB1, the K49E replacement appears to dominate the thermodynamics of the

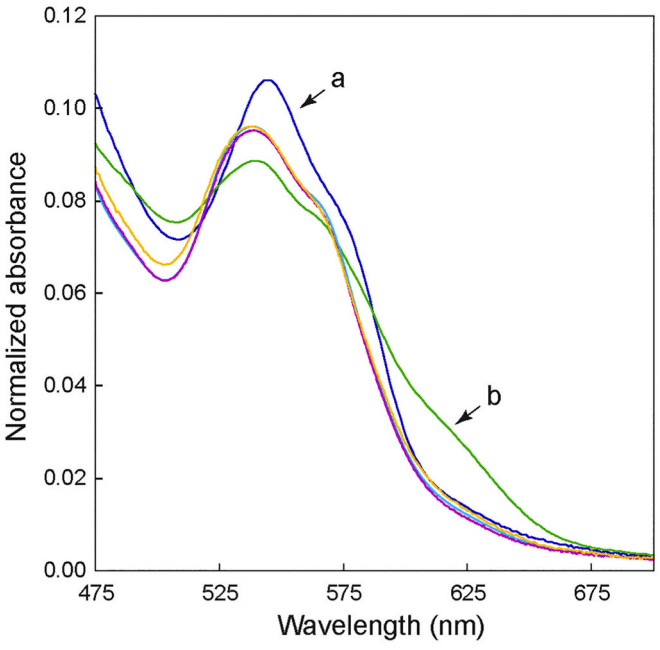

Fig. 7. Visible region of the electronic absorption spectrum of THB1 and variants at alkaline pH, after normalization of the Soret absorbance maximum to an intensity of 1. The His–Fe–OH^- spectra of K53R THB1 (a, blue) and K53A THB1 (b, green) have distinct features, while WT (cyan), R52E (magenta) and K49E/R52E (yellow) overlap as His–Fe–Lys complexes. The spectra of other variants also overlap with R52E THB1 and were omitted for clarity (Fig. S9). (For interpretation of the references to colour in this figure legend, the reader is referred to the web version of this article.)

transition. The differential populations are in good agreement with the pH responses described below (Section 3.5). The spectrum of D46L THB1 is the most affected of the aquomet spectra compared to WT and also exhibits slow exchange between water-bound and Lys-on states.

In the cyanomet state of TrHb1s, the hydroxyl group of Tyr B10 forms an H-bond to cyanide and is therefore covalently connected to the paramagnetic center. This interaction shifts the proton resonance downfield, beyond 20 ppm [67,68]. The same effect is observed in WT THB1, which has Tyr29 OηH at ~26 ppm [5]. In each of the variants containing Tyr29, the OηH signal is detected downfield (Fig. S6), confirming the formation of the H-bond to cyanide. Resolved heme resonances occur close to their counterparts in WT THB1, indicating a conserved heme pocket structure. FII THB1 also binds cyanide as determined by electronic absorbance (data not shown), but its NMR spectra before and after addition (Fig. S7) are distinct from those of all other variants. We attribute this to the absence of the H-bond network and a markedly different heme environment.

We have shown by NMR spectroscopy that Fe(III) WT THB1 undergoes lysine decoordination and water binding under moderate hydrostatic pressure [10]. This response was used for further comparative purposes. Application of increasing hydrostatic pressure to samples of K49E and R52E THB1 at a pH halfway in the Lys-on/Lys-off transition increased the intensity of hyperfine-shifted signals attributed to the aquomet state (Fig. S8). These observations support a behavior common with the WT protein.

3.5. pH titrations—Fe(III) state

The effects of THB1 modifications on the Lys-on/Lys-off equilibrium in the Fe(III) state were probed with pH titrations monitored by electronic absorption spectra. Beside the transition from the aquomet (or 5c) state to the Lys-on state, acid denaturation (pH < 5) was also observed, sometimes accompanied by a large degree of scattering. At highly basic pH (> 11), spectral changes due to tyrosine ionization, base-induced unfolding, and heme loss occurred. As a result, pH values between ~5.5 and ~11 were typically used for data collection and analysis. Exceptions are FII THB1, which displayed heme loss at pH > 10, and D46L THB1 which displayed excessive scattering at pH < 6. SVD of absorbance-versus-pH data followed by global fitting of the significant vectors (Fig. S9) yielded the apparent pK_a and Hill coefficient values reported in Table 4. The pH titration of DME-THB1, EE THB1, and FII THB1 are shown in Fig. 8 as representative examples.

Table 4
Apparent pK_a and Hill coefficients for pH-dependent heme coordination transitions in THB1 variants.

Protein	pK_a	n	Coordination equilibria
Fe(III)[a]			
WT	6.48 ± 0.07[c] (6.40 ± 0.05)	0.86 ± 0.03[c] (0.65 ± 0.03)	His/H_2O ⇌ His/Lys
WT-DME	6.75 ± 0.02	0.80 ± 0.02	His/− & His/H_2O ⇌ His/Lys
D46L	7.41 ± 0.01 (7.22 ± 0.01)	0.78 ± 0.01 (0.95 ± 0.01)	His/H_2O[d] ⇌ His/Lys
K49E	8.39 ± 0.01 (8.09 ± 0.01)	0.84 ± 0.02 (0.92 ± 0.02)	His/H_2O ⇌ His/Lys
R52E	7.71 ± 0.02 (7.60 ± 0.02)	0.75 ± 0.02 (0.87 ± 0.02)	
K49E/R52E	9.19 ± 0.01 (8.51 ± 0.01)	0.91 ± 0.01 (0.91 ± 0.02)	
Y29F	6.82 ± 0.05[c]	0.97 ± 0.05[c]	
Y29F/Q50I/Q54I	6.48 ± 0.01	0.89 ± 0.01	His/− ⇌ His/Lys
Fe(II)[b]			
WT	~6.6[c]	ND[c]	−/− & His/− ⇌ His/Lys
WT-DME	8.61 ± 0.02	0.87 ± 0.04	His/− ⇌ His/Lys
D46L	8.45 ± 0.03	0.82 ± 0.04	
K49E	9.02 ± 0.03	1.03 ± 0.07	
R52E	8.24 ± 0.03	0.81 ± 0.04	
K49E/R52E	9.68 ± 0.03	0.86 ± 0.06	
Y29F/Q50I/Q54I	8.11 ± 0.04	0.78 ± 0.05	

Determined by SVD of optical spectra and global fitting (Fig. S9 and S12). All data collected at room temperature.
ND, not determined.
[a] Performed in 5 mM phosphate (values in parentheses are for titrations with added 0.5 M KCl).
[b] Performed in different 100 mM buffers (see Section 2.1.3).
[c] From [5].
[d] Evidence of altered aquomet coordination and/or heterogenous heme binding.

The apparent pK_a of DME-THB1 (Fig. 8A,C) is close to the WT THB1 value (6.75 versus 6.5). However, on close inspection of the low-pH spectral component, it appears that this protein populates a mixture of aquomet state (with the features of R52E THB1) and a 5c state (with the features of FII THB1) in a 45:55 ratio (Fig. S10). This partitioning introduces an additional equilibrium constant, K_{OH2}, and a fractional correction for protein with water bound. When taken into account, the adjustment lowers the pK_a to 6.4. Regardless of this minor adjustment, it appears that the negative charges of the heme carboxylates do not have a strong differential effect on the Lys-on and Lys-off conformations.

The single variants K49E and R52E have apparent pK_a values of 8.4 and 7.7, respectively, for the transition to the Lys-on state. These values represent upward shifts of 1.9 and 1.2 pH units compared to WT THB1. The EE replacement raises the apparent pK_a to 9.2 (Fig. 8D,F), a 2.7 pH unit shift practically within error of the sum of individual shifts. The D46L THB1 variant behaves similarly to R52E THB1 with an upward shift of 0.9 pH unit to an apparent pK_a of 7.4. However, its low-pH spectral component determined by SVD displays a broad, blue-shifted Soret band, and cannot be deconvoluted into aquomet and 5c components like in DME-THB1. These features suggest heterogeneous heme binding or an aquomet complex with an altered coordination sphere compared to WT THB1. Finally, the FII THB1 variant is the most unusual: despite existing as a 5c complex at low pH, it has an unchanged apparent pK_a of 6.5 (Fig. 8G,I).

To investigate the electrostatic origin of some of the apparent pK_a shifts discussed above, several titrations were repeated in the presence of 0.5 M KCl (Table 4) as a non-specific, ionic screening agent. Although KCl narrows the useful range of pH by promoting precipitation, electronic absorption data suggest that the apparent pK_a of WT THB1 is barely affected at this salt concentration. Of the two single Glu variants, K49E THB1 shows a larger salt effect (−0.3 unit), whereas the EE variant displays a significant decrease from an apparent pK_a of 9.2 to 8.5, a downward shift slightly larger than the sum of the two individual shifts (0.4 pH unit). In addition, all THB1 variants tested under high ionic strength have higher fitted Hill coefficients closer to 1, indicating apparent screening of other electrostatic interactions.

3.6. pH titrations—Fe(II) state

The titration of the Fe(II) state of THB1 is challenging because of slow equilibration, limited lifetime of the reduced state, and possible transition to a 4c state [69]. For example, the WT value of 6.6, though consistent with populations detected optically and by NMR spectroscopy, is determined with less precision and accuracy than the Fe(III) value. Depending on the buffer system, the pH range that can be covered varies and can bias the result. Some of the difficulties are illustrated in Fig. S11 with the Glu variants below neutral pH. Whenever possible, data in the 5c-to-4c transition were eliminated from the pK_a determination. Regardless of these experimental limitations, all THB1 variants display interpretable transitions between common states. At pH near neutral, equilibrated proteins display high-spin spectra indicative of a 5c species (Fig. 8B,E,H). Conversion of the 5c state to the Lys-on state occurs with an elevated apparent pK_a value compared to Fe(II) WT THB1 and their respective Fe(III) states (Table 4, Fig. S12). Fe(II) DME-THB1 stands out with an increase of ~1.9 pH unit compared to Fe(III) DME-

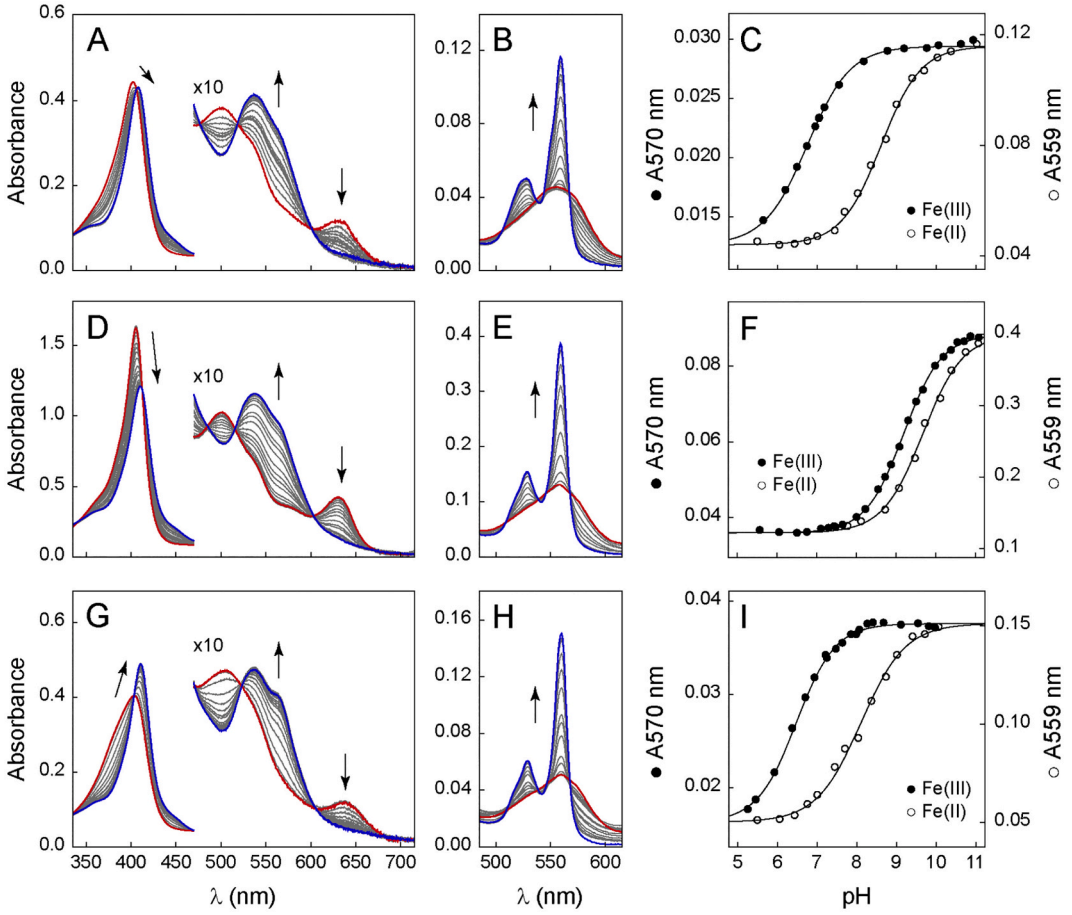

Fig. 8. Example pH titrations as monitored by electronic absorption spectroscopy. A-C: DME-THB1 with Fe(III) pK_a of 6.75 ± 0.02 and Fe(II) pK_a of 8.61 ± 0.02. D-F: K49E/R52E THB1 with Fe(III) pK_a of 9.19 ± 0.004 and Fe(II) pK_a of 9.68 ± 0.03. G-I: FII THB1 with Fe(III) pK_a of 6.48 ± 0.01 and Fe(II) pK_a of 8.11 ± 0.04. The leftmost column shows the Fe(III) state titrations, the middle column shows the Fe(II) state titrations, and the rightmost column shows fits to single wavelength data using the globally fitted parameters. Arrows indicate the direction of changes with increased pH. Complete spectral data sets and fitted values are provided in Fig. S9 and S12 and Table 4.

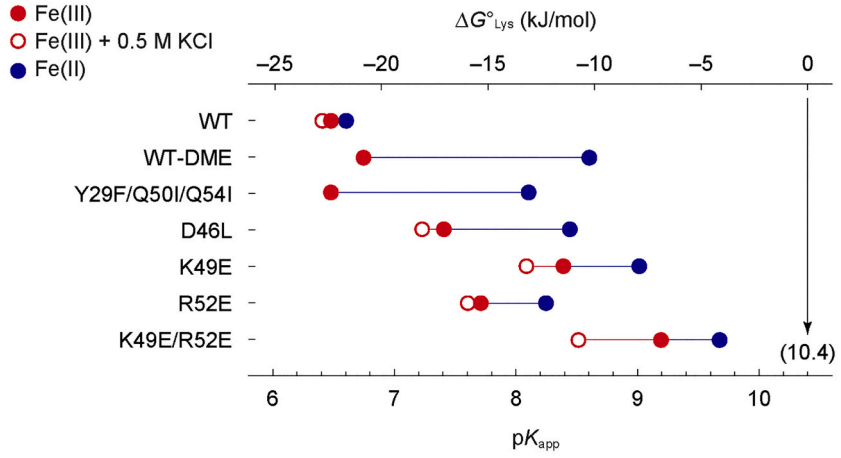

Fig. 9. Summary of the apparent Lys-on/Lys-off pK_a values reported in Table 4. The axis at the top is scaled to the pH axis and represents the stabilization free energy to maintain a coordinated lysine relative to a solvent-exposed lysine (pK_a = 10.4 [15]) in a 5c or water-coordinated protein. Uncertainties are within the symbols.

THB1. The next largest redox-dependent shifts are detected for FII and D46L THB1 (~1.6 and ~1 pH units, respectively), while the Glu replacement variants have an average increase of ~0.5 pH unit. The results are summarized in Fig. 9 and Fig. S13.

3.7. Molecular dynamics simulations

MD simulations were performed to obtain structural and dynamical information that characterizes THB1 beyond the view provided by crystal structures of the WT protein. To inspect the features of a general

Lys-off state, we used the Fe(III) cyanide-bound structure (PDB ID 6CII) as a starting point. In this simulation, the overall Lys-off conformation is maintained although individual interactions display a wide range of motions (Fig. S14). For example, the buried H-bond between the Tyr29 (B10) hydroxyl group and cyanide remains intact over 300 ns, while the Asp46 E helix N-cap displays rapid fluctuations. As anticipated, the protonated Lys53 (E10) maintains its charged amino group near the 7-propionate in a position close to that in the crystallographic structure. Lys49 (E6) and Arg79 (F10) occasionally contact the 6-propionate, whereas during the MD simulation, Arg71 (F2) and Tyr68 position their side chains to form a stable set of 7-propionate/EF loop interactions not observed in the crystal structure (Fig. S14C). Such differential arrangement of propionate H-bonding corresponds to the largely constant Cα–Cβ–Cγ–O dihedral of the 7-propionate group compared to that of the 6-propionate group, which rotates freely throughout the simulation. The headgroup of Arg52 (E9) is too far away to establish contact with the heme and instead has sustained interactions with Glu22 (B3), which in structure 6CII adopts two rotameric states in nearly equal proportions. In the time scale of the simulation, the protein does not deviate significantly from the X-ray structure (Fig. S15A).

To generate THB1 in the 5c Fe(II) state, the cyanide molecule was removed from the original model prior to equilibration. The 300-ns trajectory then shows a behavior similar to that of the cyanomet complex, including both the expected and novel polar interactions described above and largely stable backbone conformation (Fig. S15B). This result supports the short-term rigidity of the reduced state in the absence of a distal ligand and the use of 6CII as a Fe(II) Lys-off structural model (Section 3.2).

To help in explaining the measured pK_a shifts and the role of lysine ionization, MD simulations of the THB1 variants were also performed using the Fe(III) lysine-bound structure of WT THB1 (PDB ID 4XDI) as a starting point. For one set of simulations, the structure was first equilibrated with a decoordinated and neutral Lys53. The R52E, D46L, and FII replacements caused minimal backbone and side-chain perturbations, whereas the K49E and EE replacements resulted in the transient reorientation of Lys53 away from the heme pocket and out into solvent (not shown). This strongly suggests that the disruption of the Lys49 interaction with the heme propionate facilitates the transition toward the Lys-off state. When the simulations start with a decoordinated and protonated Lys53, however, all variants undergo larger amplitude changes from the Lys-on native structure. In each of the trajectories of the Glu variants, Glu49 (E6) and Glu52 (E9), if present, maintain their carboxylate group exposed to solvent. Prior to the expulsion of Lys53, D46L, FII, and R52E THB1 populate a common “Lys-in” state (Lys53 Nζ–Fe distance ~4 Å, Fig. S15C,D,F) resembling the Mb conformation with a buried E7 residue (Fig. 1B). In contrast, K49E and EE THB1 both display altered “Lys-in” conformations with slightly longer Lys53Nζ–Fe distances (~6 Å, Fig. S15E,G), suggesting a common behavior driven by the Glu49 (E6) replacement.

Both secondary structure perturbations and close-range side chain interactions formed along the trajectories brought useful insight. As expected, most of the Cα deviations observed when the protonated Lys53 exits the heme cavity are located in the E helix (Fig. S15C–G). In K49E THB1, for example, the E helix N-terminal 3_{10} turn loses its cap and unfolds as the freed Asp46 reaches the amino headgroup of the decoordinated Lys53; a tripartite interaction (Asp46–Lys53–6-propionate) persists over several ns. Arg52, when present, is able to maintain its H-bonding interaction with the 7-propionate even when Lys53 exits the heme cavity, which forces large E helix distortions. This illustrates the complex network of electrostatic interactions generated by the charge reversal substitutions. Interestingly, the D46L variant with coordinated Lys53 does not show fluctuations of the E helix over the simulation time (not shown), but when Lys53 is decoordinated severe distortions of the first turn occur transiently. Finally, although expulsion of Lys53 to solvent does occur in some of the MD simulations, such transition does not result in the canonical Lys-off state illustrated by the cyanide bound structure: the H-bonding trio of distal residues B10/E7/E11 is not generated and the B/E interhelical packing (Fig. S3) is not reconfigured. Of all the tested variants, EE THB1 has an E helix Lys-off conformation that is closest to that in 6CII at the end of the simulation and emphasizes electrostatic effects.

4. Discussion

Multiple factors influence distal heme ligation in hemoglobins and the ability of the protein to perform its function. With regards to endogenous 6c states, tertiary structure rigidity [70] and quaternary structure interfaces [71] are known determinants that can be altered with the replacement of a single or a few residues. In contrast, the role of protein side chains at the heme periphery, which control access to the heme iron and interactions with redox partners, are less well understood. In this work, we identified interactions influencing His–Fe–Lys coordination in THB1.

4.1. The structure of cyanomet THB1

The PDB hosts several structures of cyanomet TrHb1s (Table S3), which, when compared to each other, show a nearly constant distal heme environment. Cyanomet THB1 is no exception and reinforces the common features presented by these other structures. MD simulations starting with equilibrated 6CII coordinates support the resilience of the conformation. An equally stable structure is observed in simulations of the 5c Fe(II) state obtained by removal of the cyanide ligand and adjustment of the oxidation state of the iron. Most interactions expected on the basis of the crystal structure of the Lys-off state (Table S2) are maintained throughout, but the simulations also reveal some lability, as exemplified by the highly fluctuating Asp46 (E3) N-cap. New interactions are also established, such as a network involving the heme 7-propionate, Lys53, Tyr68, and Arg71.

The distal network established in cyanomet THB1 has been studied through replacements of Tyr B10 and Gln E11 in *M. tuberculosis* HbN [64] and *Tetrahymena pyriformis* trHb [72]. These variants have altered ligand affinity but give rise to conformationally similar distal pockets. An interesting deviation from standard distal side properties is provided by the recently described cyanomet *C. reinhardtii* THB11 (PDB ID 6TD7 [73]), a protein with a leucine at E7, a lysine at E10, and only 32% identity with THB1. In THB11, side chain/main chain hydrogen bonds involving two rotameric states of Ser E12 introduce a kink in the E helix, and the distal H-bond network is not formed. Lys E10 is exposed to solvent and points toward one of the heme propionates in this structure as well, whereas in the absence of cyanide, the Fe(III) electronic absorption spectrum shows signs of an endogenous 6c state. It is possible that the E helix distortion contributes to the lability of lysine coordination in this protein.

4.2. Modulation of lysine coordination in Fe(III) THB1

Static structural information, as presented by the Lys-on and Lys-off X-ray structures, raises the question of heme propionic acid dissociation. When these groups are exposed to solvent, their pK_a is 4.5–4.9 [74,75]. The value is linked to iron oxidation state and is lower in Fe(III) than in Fe(II) [76]. In a protein, local features such as hydrogen bond status and nearby charges can alter the dissociation constants. For reasons of linewidth and overlap, assignment of the heme propionate ^{1}H resonances could not be systematically achieved, and thus the propionic pK_as are currently undetermined in all states of the protein. Here, we assumed that the values are below neutral, i.e., outside of the Lys-on/Lys-off transition, because of the apparent formation of salt bridges or exposure to solvent. Accordingly, the heme propionate side chains each carry a negative charge in the MD simulations.

The single K49E and R52E replacements, by introducing charge reversals in the vicinity of the heme propionates, caused substantial

perturbation of the THB1 conformational equilibrium in the Fe(III) state, corresponding to ~11 and ~7 kJ/mol losses in apparent standard free energy of stabilization, respectively, for Lys53 coordination compared to WT THB1. The MD simulations of the Glu variants display distorted E helical structure related to the exit of Lys53 from the heme cavity, especially in EE THB1 whose large, prolonged E helix RMSD fluctuations suggest an unstable Lys-on starting conformation, presumably due to the reversal of charges at positions E6 and E9 and unfavorable repulsions near the heme propionates. We note that, although in all variants a protonated Lys53 exits the heme cavity and becomes exposed to solvent, only K49E and EE THB1s undergo a similar structural change when Lys53 is initially set to the neutral state. These two variants also exhibit the highest apparent pK_a shifts in the Fe(II) or Fe(III) state. Importantly, while the solvent exposure of Lys53 (in either ionization state) observed in our simulations does not result in the Lys-off state represented by the cyanomet 6CII structure, the range of responses surveyed here bring to light the range of fluctuations and conformational changes that (un) favorable heme propionate-protein interactions can effect.

Addition of KCl to a concentration of 0.5 M had little to no influence on the pK_a of the Lys-on/Lys-off transition in Fe(III) WT THB1 and the single Glu variants. The weak response of these THB1s to salt indicates that electrostatic interactions stabilizing one conformation over the other are either not screenable or not present. Surface salt bridges may be relatively insensitive to screening [77,78], and we favor the former interpretation. However, for the EE variant, the pK_a shift observed in the absence of added salt is significantly attenuated. We propose that this is the result of screening the repulsion between the negative charges of the heme propionates and the pair of Glu carboxylates. The repulsion would disfavor the Lys-on state (raise the apparent pK_a from the WT value) in relation to the Lys-off state, and salt would lessen the effect (raise the apparent pK_a to a lesser extent). The data emphasize the role of the heme propionates, but in light of the DME data, in the context of a negatively charged protein periphery.

Propionate esterification is expected to weaken electrostatic interactions with neighboring residues of the E and F helices, in both the Lys-on and Lys-off states and in both oxidation states. Besides eliminating the charge–charge contribution, methyl esters are hydrogen bond acceptors utilizing the carbonyl group [79] and they distort local geometry compared to the carboxylate group. The WT structures display a greater number of E helix interactions with heme propionates in the Lys-on state than in the Lys-off state, and the predicted consequence of carboxylate esterification would be a relative destabilization of the Lys-on state, i.e., an increase in the apparent pK_a of the transition. The observed effect is in the predicted direction but small compared to WT THB1 (Table 4). In contrast to the small effect on Lys ligation, the nearly equimolar mixture of aquomet and 5c species discerned by deconvolution of the Lys-off spectrum (Fig. S10) indicates the influence of the heme propionates on the ligand binding properties of the protein.

FII THB1 is similar to DME-THB1 in that it shows only a small change in apparent pK_a and has an oxidized state absorption spectrum at pH < pK_a that contrasts with the WT and Glu variants (Table 3). Fe(III) FII THB1 illustrates compensatory effects, hydrophobic interactions within the cavity counteracting the absence of coordinated water and its H-bond network. Together with D46L THB1, FII THB1 and DME-THB1 suggest that the energetic influence of variable water coordination is readily balanced by other interactions. Considering the Fe(III) data alone, the heterogeneity in Lys-off states (with full, partial, or no water coordination) complicates direct energetic comparisons to WT THB1. In relation to the Fe(II) data, however, it is possible to gain some insight into competing equilibria.

4.3. Linkage between lysine protonation, water coordination, and redox potential

Lysine is an unusual heme ligand and few model compounds are available from which to draw conclusions [80,81]. Under certain conditions, cytochrome *c* forms His-Fe-Lys complexes, but these are not well suited for systematic investigation in both oxidation states ([62] and references therein). Of interest to THB1 are studies of the binding of lysine (as a free amino acid) to microperoxidase 8 (MP8), which show a four-fold higher affinity for Fe(III) than Fe(II) at high pH [82]. Lower ratios of affinities have been reported for other nitrogenous ligands: 1.6 for imidazole and 1.1 for alanine to acetylated MP8 [83], and 1.3 for N-α-acetyllysine to acetylated MP8 [84]. FII THB1 offers a complementary and useful perspective. In both the Fe(II) and Fe(III) states, the pH-induced transition is between a 5c state and a Lys-on state. Assuming that two equilibria summarize the energetics, one written as His-Fe + Lys ⇆ His-Fe-Lys (with association constants K_2 or K_3 according to the state of the iron) and the other as $LysH^+ \leftrightarrows Lys + H^+$ (with dissociation constant $K_{out,K}$ set to $10^{-10.4}$), the apparent binding constant for neutral lysine to the heme iron is the ratio of the measured apparent $K_{a,i}$ obtained at pH below 10.4 to $K_{out,K}$ (Eq. S3). For FII THB1, the association constant in the Fe(II) state is estimated at $K_2 \sim 200$ and in the Fe(III) state at $K_3 \sim 8000$. Because the experiment does not distinguish between neutral Lys inside the heme pocket or exposed to solvent, the association constants necessarily include a protein conformational contribution; and because this contribution is expected to be independent of oxidation state, FII THB1 reports a 40-fold increase in Lys affinity on oxidizing the iron.

At pH below 10.4, the apparent pK_as of the Fe(II) proteins reflect Lys decoordination, protonation, and conformational changes. The two extremes, WT THB1 and EE THB1, bracket a 1000-fold range of apparent

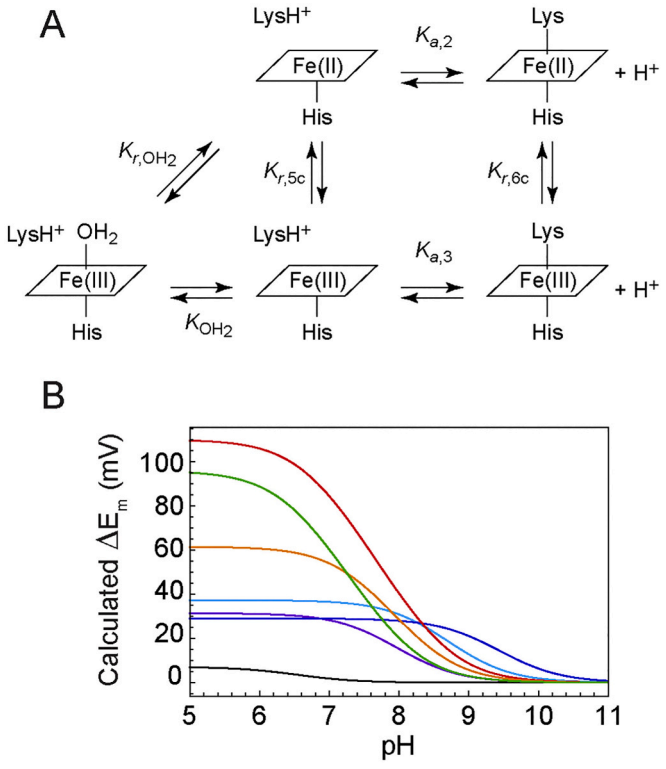

Fig. 10. A: Thermodynamic cycle relating relevant states and equilibrium constants. FII THB1 does not visit the aquomet species shown at bottom left. For other modified THB1s, reduced and oxidized iron have different sets of ligands, and water association, K_{OH2}, is included. Additional information is in the Supplementary Material. B: pH dependence of the apparent standard redox potential difference between the value at any pH and the alkaline limit and defined as $\Delta E_m = \frac{RT}{nF} ln \frac{1+10^{(pK_{a,2}-pH)}}{1+10^{(pK_{a,3}-pH)}}$ ($n = 1$). The various THB1s are WT, black; WT-DME, red; D46L, orange; K49E, cyan; R52E, purple; EE, blue; FII, green. (For interpretation of the references to colour in this figure legend, the reader is referred to the web version of this article.)

equilibrium constants. In contrast, the apparent pK_as of the Fe(III) proteins include water binding and span a 500-fold range. Assuming that the 40-fold increase in Lys affinity on iron oxidation derived from FII THB1 data holds systematically across the set of proteins, the result from FII THB1 can be extrapolated to estimate the range of water affinities in WT THB1 and variants. For WT THB1, competition between Lys53 and H_2O nearly counteracts the 40-fold effect and amounts to a K_{OH2} of ~32 or $K_d \approx 1.7$ M. For the Glu replacement variants, each of which populates the aquomet state, the average K_{OH2} is 9.7 ± 1.4 and corresponds to a $K_d \approx 5.7$ M. These values are considerably larger than the water dissociation constant reported for Mb ($K_d = 61$ mM [85]), but apparently reaching a very high value for FII THB1. The interplay of water and lysine affinities is illustrated in Fig. S16 and S17.

By a simplified thermodynamic cycle [86] (Fig. 10A), the apparent standard redox potential of the Lys-on and Lys-off states of WT THB1 would be close to each other and to the measured −67 mV at pH 7 [17]. This value favors the Fe(II) state in the reducing and buffered cytosol of *C. reinhardtii* [87]. In contrast to WT THB1, each of the modified proteins has an apparent pK_a measurably higher in the Fe(II) than the Fe(III) state (Table 4, Fig. 9). The modified proteins are therefore expected to show a difference in the redox potential of the two ligation states. Fig. 10B summarizes the pH-dependence of the apparent redox potential difference, ΔE_m, calculated on the basis of the apparent pK_as. The modified THB1s can be divided in two groups according to the size of ΔE_m, whether smaller or larger than 50 mV. The first group ($\Delta E_m < 50$ mV) contains the Glu variants. Surface charges can affect the redox potential to the extent observed here [88–90] and a similar influence is likely at work for these proteins. The second group ($\Delta E_m > 50$ mV) contains D46L, DME, and FII THB1, proteins discussed above as having altered or abolished water coordination.

4.4. Primary structure considerations

The data presented here illustrate that, in the particular background of THB1, simultaneous charge reversal replacements at Lys49 (E6) and Arg52 (E9) have the most destabilizing and nearly additive effect on the Lys-on state. There are now thousands of TrHb1 sequences available in curated databases. Although progress has been made through homology-based strategies [91], distal coordination cannot be predicted reliably. Characterization of each protein is clearly impractical, which justifies the need for identifying potential coordination determinants. A multiple sequence alignment of 1,047 TrHb1s [66] revealed over 300 instances of Lys E10, and within this group, the preponderance of Ala (> 40%) and low frequency of Arg (< 6%) at position E9, and the preponderance of Arg (~40%) followed by Lys (~24%) and with few Ala (< 10%) at E6. Experimental data describing heme coordination in the Fe(III) and Fe(II) states of these extant proteins are largely unavailable, and for the few characterized TrHbs that have a lysine at E10, there is no simple correlation between the identity of the residues at E6 and E9 and the strength of lysine coordination relative to water [17]. Nevertheless, the compositional distribution at these E helix positions, where residues can interact with the heme, does support the existence of control points for the response of TrHb1s to changes in pH and redox status of the environment. This aspect of THB1 is pursued further with Ala replacements in the accompanying paper (Julió Plana et al., submitted).

The structural data presented here also hint at additional determinants. Among TrHb1s, structural variations have been noted on the proximal side, with an F helix that extends for just one turn (e.g., in *C. eugametos* TrHb1, PDB ID 1DLY [50]), three irregular turns (e.g., in *C. reinhardtii* THB1, PDB ID 6CII), or four irregular turns (e.g., in the *bis*-His state of *Synechococcus* GlbN [55]). The EF and FG loops are regions containing amino acid insertions in TrHb1 sequences, which exacerbates differences among proteins (Fig. S18). Sequence and structure alignments show position F10 (Arg79 in THB1) to be variable although position F2 (Arg71 in THB1) shows a preference for Lys/Arg with a tendency to point to a heme propionate in exogenous 6c states. The participation of these side chains and the impact of F helix variations in conformational stabilization cannot be ignored. In addition to heme propionate-protein interactions, the results implicate the rearrangement of interhelical packing on ligand binding (Fig. 5) and the integrity of the E helix, structural factors that tend to be well conserved within TrHb1s and applicable to most members of the family, not only for those displaying endogenous distal coordination.

4.5. pH-dependent conformational changes

The Lys-on/Lys-off process is a pH-driven conformational change linked to heme coordination. In that, it shares similarities with the pH-controlled O_2 affinity of multimeric hemoglobins [1,92] (Bohr effect) and the pH-controlled NO affinity of nitrophorin 4 (NP4) [93–95]. Whereas in these examples of heterotropic allostery the protonation site is remote from the heme, and the pH of the environment varies, in THB1, the trigger is the axial ligand itself, and the pH of the alga cytoplasm is well buffered at ~7.4 [96]. We have proposed that the formation of the endogenous 6c complex in THB1 facilitates the reduction of the heme iron after it has donated an electron for the conversion of NO into nitrate [10]. In this view, WT THB1's apparent pK_a of ~6.5 in both Fe(III) and Fe(II) oxidation states has physiological significance. However, the aerobic enzymatic activity requires O_2 diffusion into the distal site and binding, presumably in the Lys-off (5c) conformation, represented by the cyanomet structure presented in this work. The modifications we explored here, located at the periphery of the heme cofactor, appear to perturb an otherwise optimized arrangement of interactions that balance two conformational states useful for THB1 function. Another consequence linked to the Lys-on/Lys-off transition and exposed by the new structure is a change in surface electrostatics. Compared to other TrHb1s, the presence of positively charged residues at E6 and E9 emerges as a possible strategy to adjust interactions with a cognate reductase and enzymatic activity within the cell.

5. Conclusion

Over the range of physiological pH (7.3–7.5, [96]) the population of the endogenous 6c state of WT THB1 varies by a few percent (83–88). Because the apparent pK_as of the Fe(II) and Fe(III) protein are close to each other, the pH variation does not cause a change in redox potential. Such properties are advantageous to maintain THB1 in an active state for the efficient management of cellular NO. A preliminary interpretation of X-ray structures leads to the hypothesis that the differential formation of salt bridges involving the heme propionates plays a role in positioning the equilibrium between endogenous 6c and exogenous 6c or 5c coordination schemes and adjusting the redox potential of the heme group. Indeed, we found that engineering repulsions between heme propionates and protein scaffold was effective at destabilizing the Lys-on state, both in the Fe(III) and the Fe(II) states, and more in the latter than in the former. Heme propionate neutralization did have a differential effect on the two redox states but acted solely on the reduced state in a confirmation of participation of the heme carboxylates in setting the potential. Elimination of the distal H-bond network, while abrogating distal water coordination in the Fe(III) state, had a net influence similar to that of heme propionate esterification by affecting principally the reduced state transition. Finally, tempering with the E helix N-cap resulted in perturbations of both oxidation states resembling the charge reversal effects. The differential alterations reflect a balance of influences readily upset by the modification of the heme periphery. The replacements discussed here emphasize that the pH- and redox-sensing capability of a truncated hemoglobin can be manipulated over a broad range of values. The study also provides a framework with which to anticipate the properties of arbitrary TrHb sequences.

Declaration of Competing Interest

The authors declare that they have no known competing financial interests or personal relationships that could have appeared to influence the work reported in this paper.

Acknowledgments

The authors thank Dr. Matthew Preimesberger for assistance in purification, NMR and pH titration data collection of K49E THB1; Dr. Selena Rice for purification of D46L THB1 and collection of its Fe(III) pH titration; Dr. Maxime Siegler for X-ray data collection; and Dr. Eric Johnson for assistance throughout the study.

This research was supported by grants from the Universidad de Buenos Aires (UBACYT 20020120300025BA), Agencia Nacional de Promoción Científica y Tecnológica (PICT 2012-2571, PICT 2014-1022, and PICT 2015-2761) and CONICET Grant 11220150100303CO. L.J.P. holds a CONICET PhD fellowship. D.A.E. and L.C. are members of CONICET. Support was also provided by the National Science Foundation grant numbers MCB-1330488 and CHE-2003950 to J.T.J.L. and GRFP-1746891 to J.E.M.G.

Appendix A. Supplementary data

Supplementary data to this article can be found online at https://doi.org/10.1016/j.jinorgbio.2021.111437.

References

[1] D.A. Gell, Structure and function of haemoglobins, Blood Cells Mol. Dis. 70 (2018) 13–42, https://doi.org/10.1016/j.bcmd.2017.10.006.
[2] D. de Sanctis, P. Ascenzi, A. Bocedi, S. Dewilde, T. Burmester, T. Hankeln, L. Moens, M. Bolognesi, Cyanide binding and heme cavity conformational transitions in *Drosophila melanogaster* hexacoordinate hemoglobin, Biochemistry. 45 (2006) 10054–10061, https://doi.org/10.1021/bi060462a.
[3] E.A. Johnson, J.T.J. Lecomte, The globins of cyanobacteria and algae, Adv. Microb. Physiol. 63 (2013) 195–272, https://doi.org/10.1016/B978-0-12-407693-8.00006-6.
[4] E.A. Johnson, J.T.J. Lecomte, Characterization of the truncated hemoglobin THB1 from protein extracts of *Chlamydomonas reinhardtii*, F1000Research. 3 (2014) 294, https://doi.org/10.12688/f1000research.5873.1.
[5] E.A. Johnson, S.L. Rice, M.R. Preimesberger, D.B. Nye, L. Gilevicius, B.B. Wenke, J. M. Brown, G.B. Witman, J.T.J. Lecomte, Characterization of THB1, a *Chlamydomonas reinhardtii* truncated hemoglobin: linkage to nitrogen metabolism and identification of lysine as the distal heme ligand, Biochemistry. 53 (2014) 4573–4589, https://doi.org/10.1021/bi5005206.
[6] E. Minaeva, Z. Zalutskaya, V. Filina, E. Ermilova, Truncated hemoglobin 1 is a new player in *Chlamydomonas reinhardtii* acclimation to sulfur deprivation, PLoS One. 12 (2017), e0186851, https://doi.org/10.1371/journal.pone.0186851.
[7] V. Filina, A. Grinko, E. Ermilova, Truncated hemoglobins 1 and 2 are implicated in the modulation of phosphorus deficiency-induced nitric oxide levels in *Chlamydomonas*, Cells. 8 (2019) 947, https://doi.org/10.3390/cells8090947.
[8] Z. Zalutskaya, L. Kochemasova, E. Ermilova, Dual positive and negative control of *Chlamydomonas* PII signal transduction protein expression by nitrate/nitrite and NO via the components of nitric oxide cycle, BMC Plant Biol. 18 (2018) 305, https://doi.org/10.1186/s12870-018-1540-x.
[9] C.M. Bellido-Pedraza, V. Calatrava, E. Sanz-Luque, M. Tejada-Jiménez, Á. Llamas, M. Plouviez, B. Guieysse, E. Fernández, A. Galván, *Chlamydomonas reinhardtii*, an algal model in the nitrogen cycle, Plants. 9 (2020) 903, https://doi.org/10.3390/plants9070903.
[10] M.R. Preimesberger, A. Majumdar, J.T.J. Lecomte, Dynamics of lysine as a heme axial ligand: NMR analysis of the *Chlamydomonas reinhardtii* hemoglobin THB1, Biochemistry. 56 (2017) 551–569, https://doi.org/10.1021/acs.biochem.6b00926.
[11] R.A. Marcus, N. Sutin, Electron transfers in chemistry and biology, Biochim. Biophys. Acta. 811 (1985) 265–322.
[12] C.J. Reedy, B.R. Gibney, Heme protein assemblies, Chem. Rev. 104 (2004) 617–649, https://doi.org/10.1021/cr0206115.
[13] C.J. Reedy, M.M. Elvekrog, B.R. Gibney, Development of a heme protein structure-electrochemical function database, Nucleic Acids Res. 36 (2008) D307–D313, https://doi.org/10.1093/nar/gkm814.
[14] J.H. Dawson, Probing structure-function relations in heme-containing oxygenases and peroxidases, Science. 240 (1988) 433–439, https://doi.org/10.1126/science.3358128.
[15] C.N. Pace, G.R. Grimsley, J.M. Scholtz, Protein ionizable groups: p*K* values and their contribution to protein stability and solubility, J. Biol. Chem. 284 (2009) 13285–13289, https://doi.org/10.1074/jbc.R800080200.
[16] S.L. Rice, L.E. Boucher, J.L. Schlessman, M.R. Preimesberger, J. Bosch, J.T. J. Lecomte, Structure of *Chlamydomonas reinhardtii* THB1, a group 1 truncated hemoglobin with a rare histidine-lysine heme ligation, Acta Crystallogr. F Struct. Biol. Commun. 71 (2015) 718–725, https://doi.org/10.1107/S2053230X15006949.
[17] E.A. Johnson, M.M. Russo, D.B. Nye, J.L. Schlessman, J.T.J. Lecomte, Lysine as a heme iron ligand: a property common to three truncated hemoglobins from *Chlamydomonas reinhardtii*, Biochim. Biophys. Acta. 1862 (2018) 2660–2673, https://doi.org/10.1016/j.bbagen.2018.08.009.
[18] E.A. Berry, B.L. Trumpower, Simultaneous determination of hemes *a*, *b*, and *c* from pyridine hemochrome spectra, Anal. Biochem. 161 (1987) 1–15, https://doi.org/10.1016/0003-2697(87)90643-9.
[19] A.R. Lim, B.P. Sishta, A.G. Mauk, Contribution of the heme propionate groups to the electron transfer and electrostatic properties of myoglobin, J. Inorg. Biochem. 100 (2006) 2017–2023, https://doi.org/10.1016/j.jinorgbio.2006.08.019.
[20] T. Asakura, D.W. Lamson, Preparation of protohemin monomethyl ester, Anal. Biochem. 53 (1973) 448–451, https://doi.org/10.1016/0003-2697(73)90093-6.
[21] P.D. Adams, P.V. Afonine, G. Bunkoczi, V.B. Chen, I.W. Davis, N. Echols, J. J. Headd, L.W. Hung, G.J. Kapral, R.W. Grosse-Kunstleve, A.J. McCoy, N. W. Moriarty, R. Oeffner, R.J. Read, D.C. Richardson, J.S. Richardson, T. C. Terwilliger, P.H. Zwart, PHENIX: a comprehensive python-based system for macromolecular structure solution, Acta Crystallogr. D Biol. Crystallogr. 66 (2010) 213–221, https://doi.org/10.1107/S0907444909052925.
[22] P. Emsley, B. Lohkamp, W.G. Scott, K. Cowtan, Features and development of coot, Acta Crystallogr. D Biol. Crystallogr. 66 (2010) 486–501, https://doi.org/10.1107/S0907444910007493.
[23] C.J. Williams, J.J. Headd, N.W. Moriarty, M.G. Prisant, L.L. Videau, L.N. Deis, V. Verma, D.A. Keedy, B.J. Hintze, V.B. Chen, S. Jain, S.M. Lewis, W.B. Arendall III, J. Snoeyink, P.D. Adams, S.C. Lovell, J.S. Richardson, D.C. Richardson, MolProbity: more and better reference data for improved all-atom structure validation, Protein Sci. 27 (2018) 293–315, https://doi.org/10.1002/pro.3330.
[24] E.F. Pettersen, T.D. Goddard, C.C. Huang, G.S. Couch, D.M. Greenblatt, E.C. Meng, T.E. Ferrin, UCSF Chimera—a visualization system for exploratory research and analysis, J. Comput. Chem. 25 (2004) 1605–1612, https://doi.org/10.1002/jcc.20084.
[25] L. Pravda, D. Sehnal, D. Toušek, V. Navrátilová, V. Bazgier, K. Berka, R. Svobodová Vařeková, J. Koča, M. Otyepka, MOLEonline: a web-based tool for analyzing channels, tunnels and pores (2018 update), Nucleic Acids Res. 46 (2018) W368–W373, https://doi.org/10.1093/nar/gky309.
[26] E.W. Baumann, Determination of pH in concentrated salt solutions, Anal. Chim. Acta. 64 (1973) 284–288, https://doi.org/10.1016/S0003-2670(01)82448-X.
[27] A.D. Wiesner, L.E. Katz, C.-C. Chen, The impact of ionic strength and background electrolyte on pH measurements in metal ion adsorption experiments, J. Colloid Interface Sci. 301 (2006) 329–332, https://doi.org/10.1016/j.jcis.2006.05.011.
[28] R.W. Hendler, R.I. Shrager, Deconvolutions based on singular value decomposition and the pseudoinverse: a guide for beginners, J. Biochem. Biophys. Methods. 28 (1994) 1–33, https://doi.org/10.1016/0165-022X(94)90061-2.
[29] R.J. Quinlan, G.D. Reinhart, Baroresistant buffer mixtures for biochemical analyses, Anal. Biochem. 341 (2005) 69–76, https://doi.org/10.1016/j.ab.2005.03.002.
[30] P. Arroyo Manez, C. Lu, L. Boechi, M.A. Martí, M. Shepherd, J.L. Wilson, R. K. Poole, F.J. Luque, S.R. Yeh, D.A. Estrin, Role of the distal hydrogen-bonding network in regulating oxygen affinity in the truncated hemoglobin III from *Campylobacter jejuni*, Biochemistry. 50 (2011) 3946–3956, https://doi.org/10.1021/bi101137n.
[31] L. Capece, M.A. Martí, A. Bidon-Chanal, A. Nadra, F.J. Luque, D.A. Estrin, High pressure reveals structural determinants for globin hexacoordination: neuroglobin and myoglobin cases, Proteins. 75 (2009) 885–894, https://doi.org/10.1002/prot.22297.
[32] L. Capece, M.A. Martí, A. Crespo, F. Doctorovich, D.A. Estrin, Heme protein oxygen affinity regulation exerted by proximal effects, J. Am. Chem. Soc. 128 (2006) 12455–12461, https://doi.org/10.1021/ja0620033.
[33] U.N. Morzan, L. Capece, M.A. Martí, D.A. Estrin, Quaternary structure effects on the hexacoordination equilibrium in rice hemoglobin rHb1: insights from molecular dynamics simulations, Proteins: Struct. Funct. Bioinf. 81 (2013) 863–873, https://doi.org/10.1002/prot.24245.
[34] D.A. Case, R.M. Betz, D.S. Cerutti, T.E. Cheatham, T.A. Darden, R.E. Duke, T. J. Giese, H. Gohlke, A.W. Goetz, N. Homeyer, S. Izadi, P. Janowski, J. Kaus, A. Kovalenko, T.S. Lee, S. LeGrand, P. Li, C. Lin, T. Luchko, R. Luo, B. Madej, D. Mermelstein, K.M. Merz, G. Monard, H. Nguyen, H.T. Nguyen, I. Omelyan, A. Onufriev, D.R. Roe, A. Roitberg, C. Sagui, C.L. Simmerling, W.M. Botello-Smith,

J. Swails, R.C. Walker, J. Wang, R.M. Wolf, X. Wu, L. Xiao, P.A. Kollman, AMBER 2016, University of California, San Francisco, 2016.
[35] W.L. Jorgensen, J. Chandrasekhar, J.D. Madura, R.W. Impey, M.L. Klein, Comparison of simple potential functions for simulating liquid water, J. Chem. Phys. 79 (1983) 926–935, https://doi.org/10.1063/1.445869.
[36] J.A. Maier, C. Martinez, K. Kasavajhala, L. Wickstrom, K.E. Hauser, C. Simmerling, ff14SB: improving the accuracy of protein side chain and backbone parameters from ff99SB, J. Chem. Theory Comput. 11 (2015) 3696–3713, https://doi.org/10.1021/acs.jctc.5b00255.
[37] M.A. Martí, A. Crespo, L. Capece, L. Boechi, D.E. Bikiel, D.A. Scherlis, D.A. Estrin, Dioxygen affinity in heme proteins investigated by computer simulation, J. Inorg. Biochem. 100 (2006) 761–770, https://doi.org/10.1016/j.jinorgbio.2005.12.009.
[38] F. Forti, L. Boechi, D. Bikiel, M.A. Martí, M. Nardini, M. Bolognesi, C. Viappiani, D. Estrin, F.J. Luque, Ligand migration in *Methanosarcina acetivorans* protoglobin: effects of ligand binding and dimeric assembly, J. Phys. Chem. B. 115 (2011) 13771–13780, https://doi.org/10.1021/jp208562b.
[39] L. Capece, A. Lewis-Ballester, M.A. Martí, D.A. Estrin, S.R. Yeh, Molecular basis for the substrate stereoselectivity in tryptophan dioxygenase, Biochemistry. 50 (2011) 10910–10918, https://doi.org/10.1021/bi201439m.
[40] D. Giordano, L. Boechi, A. Vergara, M.A. Martí, U. Samuni, D. Dantsker, L. Grassi, D.A. Estrin, J.M. Friedman, L. Mazzarella, G. di Prisco, C. Verde, The hemoglobins of the sub-Antarctic fish *Cottoperca gobio*, a phyletically basal species–oxygen-binding equilibria, kinetics and molecular dynamics, FEBS J. 276 (2009) 2266–2277, https://doi.org/10.1111/j.1742-4658.2009.06954.x.
[41] L.L. Perissinotti, M.A. Martí, F. Doctorovich, F.J. Luque, D.A. Estrin, A microscopic study of the deoxyhemoglobin-catalyzed generation of nitric oxide from nitrite anion, Biochemistry. 47 (2008) 9793–9802, https://doi.org/10.1021/bi801104c.
[42] D.E. Bikiel, L. Boechi, L. Capece, A. Crespo, P.M. De Biase, S. Di Lella, M. C. Gonzalez Lebrero, M.A. Martí, A.D. Nadra, L.L. Perissinotti, D.A. Scherlis, D. A. Estrin, Modeling heme proteins using atomistic simulations, Phys. Chem. Chem. Phys. 8 (2006) 5611–5628, https://doi.org/10.1039/b611741b.
[43] M.A. Martí, L. Capece, A. Bidon-Chanal, A. Crespo, V. Guallar, F.J. Luque, D. A. Estrin, Nitric oxide reactivity with globins as investigated through computer simulation, Methods Enzymol. 437 (2008) 477–498, https://doi.org/10.1016/S0076-6879(07)37024-9.
[44] F.P. Nicoletti, E. Droghetti, B.D. Howes, J.P. Bustamante, A. Bonamore, N. Sciamanna, D.A. Estrin, A. Feis, A. Boffi, G. Smulevich, H-bonding networks of the distal residues and water molecules in the active site of *Thermobifida fusca* hemoglobin, Biochim. Biophys. Acta-Proteins Proteom. 1834 (2013) 1901–1909, https://doi.org/10.1016/j.bbapap.2013.02.033.
[45] J.-P. Ryckaert, G. Ciccotti, H.J.C. Berendsen, Numerical integration of the cartesian equations of motion of a system with constraints: molecular dynamics of n-alkanes, J. Comput. Phys. 23 (1977) 327–341, https://doi.org/10.1016/0021-9991(77)90098-5.
[46] H.J.C. Berendsen, J.P.M. Postma, W.F. Vangunsteren, A. Dinola, J.R. Haak, Molecular-dynamics with coupling to an external bath, J. Chem. Phys. 81 (1984) 3684–3690, https://doi.org/10.1063/1.448118.
[47] X. Wu, B.R. Brooks, E. Vanden-Eijnden, Self-guided Langevin dynamics via generalized Langevin equation, J. Comput. Chem. 37 (2016) 595–601, https://doi.org/10.1002/jcc.24015.
[48] W. Humphrey, A. Dalke, K. Schulten, VMD: visual molecular dynamics, J. Mol. Graph. 14 (1996) 33–38, https://doi.org/10.1016/0263-7855(96)00018-5.
[49] M. Milani, Y. Ouellet, H. Ouellet, M. Guertin, A. Boffi, G. Antonini, A. Bocedi, M. Mattu, M. Bolognesi, P. Ascenzi, Cyanide binding to truncated hemoglobins: a crystallographic and kinetic study, Biochemistry. 43 (2004) 5213–5221, https://doi.org/10.1021/bi049870+.
[50] A. Pesce, M. Couture, S. Dewilde, M. Guertin, K. Yamauchi, P. Ascenzi, L. Moens, M. Bolognesi, A novel two-over-two a-helical sandwich fold is characteristic of the truncated hemoglobin family, EMBO J. 19 (2000) 2424–2434, https://doi.org/10.1093/emboj/19.11.2424.
[51] J.A. Shelnutt, X.Z. Song, J.G. Ma, S.L. Jia, W. Jentzen, C.J. Medforth, Nonplanar porphyrins and their significance in proteins, Chem. Soc. Rev. 27 (1998) 31–41, https://doi.org/10.1039/A827031Z.
[52] D.A. Vuletich, J.T.J. Lecomte, A phylogenetic and structural analysis of truncated hemoglobins, J. Mol. Evol. 62 (2006) 196–210, https://doi.org/10.1007/s00239-005-0077-4.
[53] M.R. Preimesberger, A. Majumdar, S.L. Rice, L. Que, J.T.J. Lecomte, Helix-capping histidines: diversity of N-H…N hydrogen bond strength revealed by $^{2h}J_{NN}$ scalar couplings, Biochemistry. 54 (2015) 6896–6908, https://doi.org/10.1021/acs.biochem.5b01002.
[54] J.T. Trent 3rd, S. Kundu, J.A. Hoy, M.S. Hargrove, Crystallographic analysis of *Synechocystis* cyanoglobin reveals the structural changes accompanying ligand binding in a hexacoordinate hemoglobin, J. Mol. Biol. 341 (2004) 1097–1108, https://doi.org/10.1016/j.jmb.2004.05.070.
[55] B.B. Wenke, J.T.J. Lecomte, A. Héroux, J.L. Schlessman, The 2/2 hemoglobin from the cyanobacterium *Synechococcus* sp. PCC 7002 with covalently attached heme: comparison of X-ray and NMR structures, Proteins. 82 (2014) 528–534, https://doi.org/10.1002/prot.24409.
[56] M. Milani, A. Pesce, Y. Ouellet, S. Dewilde, J. Friedman, P. Ascenzi, M. Guertin, M. Bolognesi, Heme-ligand tunneling in group I truncated hemoglobins, J. Biol. Chem. 279 (2004) 21520–21525, https://doi.org/10.1074/jbc.M401320200.
[57] M. Milani, A. Pesce, Y. Ouellet, P. Ascenzi, M. Guertin, M. Bolognesi, *Mycobacterium tuberculosis* hemoglobin N displays a protein tunnel suited for O_2 diffusion to the heme, EMBO J. 20 (2001) 3902–3909, https://doi.org/10.1093/emboj/20.15.3902.
[58] R. Daigle, J.A. Rousseau, M. Guertin, P. Lagüe, Theoretical investigations of nitric oxide channeling in *Mycobacterium tuberculosis* truncated hemoglobin N, Biophys. J. 97 (2009) 2967–2977, https://doi.org/10.1016/j.bpj.2009.09.006.
[59] A.M. Lesk, C. Chothia, How different amino acid sequences determine similar protein structures: the structure and evolutionary dynamics of the globins, J. Mol. Biol. 136 (1980) 225–270, https://doi.org/10.1016/0022-2836(80)90373-3.
[60] E.A. Johnson, J.T.J. Lecomte, The haemoglobins of algae, Adv. Microb. Physiol. 67 (2015) 177–234, https://doi.org/10.1016/bs.ampbs.2015.08.003.
[61] F. Germani, A. Pesce, A. Venturini, L. Moens, M. Bolognesi, S. Dewilde, M. Nardini, High resolution crystal structures of the *Cerebratulus lacteus* mini-Hb in the unligated and carbomonoxy states, Int. J. Mol. Sci. 13 (2012) 8025–8037, https://doi.org/10.3390/ijms13078025.
[62] D.B. Nye, M.R. Preimesberger, A. Majumdar, J.T.J. Lecomte, Histidine–lysine axial ligand switching in a hemoglobin: a role for heme propionates, Biochemistry. 57 (2018) 631–644, https://doi.org/10.1021/acs.biochem.7b01155.
[63] K. Shikama, A. Matsuoka, Spectral properties unique to the myoglobins lacking the usual distal histidine residue, J. Mol. Biol. 209 (1989) 489–491, https://doi.org/10.1016/0022-2836(89)90012-0.
[64] Y. Ouellet, M. Milani, M. Couture, M. Bolognesi, M. Guertin, Ligand interactions in the distal heme pocket of *Mycobacterium tuberculosis* truncated hemoglobin N: roles of TyrB10 and GlnE11 residues, Biochemistry. 45 (2006) 8770–8781, https://doi.org/10.1021/bi060112o.
[65] K. Akiyama, M. Fukuda, N. Kobayashi, A. Matsuoka, K. Shikama, The pH-dependent swinging-out of the distal histidine residue in ferric hemoglobin of a midge larva (*Tokunagayusurika akamusi*), Biochim. Biophys. Acta. 1208 (1994) 306–309, https://doi.org/10.1016/0167-4838(94)90117-1.
[66] D.B. Nye, E.A. Johnson, M.H. Mai, J.T.J. Lecomte, Replacement of the heme axial lysine as a test of conformational adaptability in the truncated hemoglobin THB1, J. Inorg. Biochem. 201 (2019) 110824, https://doi.org/10.1016/j.jinorgbio.2019.110824.
[67] B.C. Vu, H.J. Nothnagel, D.A. Vuletich, C.J. Falzone, J.T.J. Lecomte, Cyanide binding to hexacoordinate cyanobacterial hemoglobins: hydrogen bonding network and heme pocket rearrangement in ferric H117A *Synechocystis* Hb, Biochemistry. 43 (2004) 12622–12633, https://doi.org/10.1021/bi048726l.
[68] S.L. Rice, M.R. Preimesberger, E.A. Johnson, J.T.J. Lecomte, Introduction of a covalent histidine-heme linkage in a hemoglobin: a promising tool for heme protein engineering, J. Inorg. Biochem. 141 (2014) 198–207, https://doi.org/10.1016/j.jinorgbio.2014.09.009.
[69] M. Couture, T.K. Das, H.C. Lee, J. Peisach, D.L. Rousseau, B.A. Wittenberg, J. B. Wittenberg, M. Guertin, *Chlamydomonas* chloroplast ferrous hemoglobin. Heme pocket structure and reactions with ligands, J. Biol. Chem. 274 (1999) 6898–6910, https://doi.org/10.1074/jbc.274.11.6898.
[70] S. Kakar, F.G. Hoffman, J.F. Storz, M. Fabian, M.S. Hargrove, Structure and reactivity of hexacoordinate hemoglobins, Biophys. Chem. 152 (2010) 1–14, https://doi.org/10.1016/j.bpc.2010.08.008.
[71] S. Kakar, R. Sturms, A. Tiffany, J.C. Nix, A.A. DiSpirito, M.S. Hargrove, Crystal structures of *Parasponia* and *Trema* hemoglobins: differential heme coordination is linked to quaternary structure, Biochemistry. 50 (2011) 4273–4280, https://doi.org/10.1021/bi2002423.
[72] J. Igarashi, K. Kobayashi, A. Matsuoka, A hydrogen-bonding network formed by the B10-E7-E11 residues of a truncated hemoglobin from *Tetrahymena pyriformis* is critical for stability of bound oxygen and nitric oxide detoxification, J. Biol. Inorg. Chem. 16 (2011) 599–609, https://doi.org/10.1007/s00775-011-0761-3.
[73] D. Huwald, S. Duda, R. Gasper, V. Olieric, E. Hofmann, A. Hemschemeier, Distinctive structural properties of THB11, a pentacoordinate *Chlamydomonas reinhardtii* truncated hemoglobin with N- and C-terminal extensions, J. Biol. Inorg. Chem. 25 (2020) 267–283, https://doi.org/10.1007/s00775-020-01759-2.
[74] J.E. Falk, Porphyrins and Metalloporphyrins, Elsevier, New York, 1964.
[75] E.P. Serjeant, B. Dempsey, IUPAC Data Series, in: Ionisation Constants of Organic Acids in Aqueous Solution, Permagon, Oxford, 1979.
[76] D.K. Das, O.K. Medhi, The role of heme propionate in controlling the redox potential of heme: square wave voltammetry of protoporphyrinato IX iron(III) in aqueous surfactant micelles, J. Inorg. Biochem. 70 (1998) 83–90, https://doi.org/10.1016/S0162-0134(98)10002-8.
[77] Y.-H. Kao, C.A. Fitch, S. Bhattacharya, C.J. Sarkisian, J.T.J. Lecomte, B. García-Moreno E., Salt effects on ionization equilibria of histidines in myoglobin, Biophys. J. 79 (2000) 1637–1654, https://doi.org/10.1016/s0006-3495(00)76414-9.
[78] D.L. Luisi, C.D. Snow, J.-J. Lin, Z.S. Hendsch, B. Tidor, D.P. Raleigh, Surface salt bridges, double-mutant cycles, and protein stability: an experimental and computational analysis of the interaction of the Asp 23 side chain with the N-terminus of the N-terminal domain of the ribosomal protein L9, Biochemistry. 42 (2003) 7050–7060, https://doi.org/10.1021/bi027202n.
[79] J.P.M. Lommerse, S.L. Price, R. Taylor, Hydrogen bonding of carbonyl, ether, and ester oxygen atoms with alkanol hydroxyl groups, J. Comput. Chem. 18 (1997) 757–774, https://doi.org/10.1002/(sici)1096-987x(19970430)18:6<757::aid-jcc3>3.0.co;2-r.
[80] J. Du, R. Perera, J.H. Dawson, Alkylamine-ligated H93G myoglobin cavity mutant: a model system for endogenous lysine and terminal amine ligation in heme proteins such as nitrite reductase and cytochrome *f*, Inorg. Chem. 50 (2011) 1242–1249, https://doi.org/10.1021/ic101644u.
[81] J. Du, M. Sono, J.H. Dawson, The H93G myoglobin cavity mutant as a versatile scaffold for modeling heme iron coordination structures in protein active sites and their characterization with magnetic circular dichroism spectroscopy, Coord. Chem. Rev. 255 (2011) 700–716, https://doi.org/10.1016/j.ccr.2011.01.029.

[82] S. Othman, A. Desbois, Resonance Raman investigation of lysine and N-acetylmethionine complexes of ferric and ferrous microperoxidase, Eur. Biophys. J. 28 (1998) 12–25, https://doi.org/10.1007/s002490050179.
[83] F.A. Tezcan, J.R. Winkler, H.B. Gray, Effects of ligation and folding on reduction potentials of heme proteins, J. Am. Chem. Soc. 120 (1998) 13383–13388, https://doi.org/10.1021/ja982536e.
[84] F. Zhong, E.V. Pletneva, Ligation and reactivity of methionine-oxidized cytochrome *c*, Inorg. Chem. 57 (2018) 5754–5766, https://doi.org/10.1021/acs.inorgchem.8b00010.
[85] W. Cao, J.F. Christian, P.M. Champion, F. Rosca, J.T. Sage, Water penetration and binding to ferric myoglobin, Biochemistry. 40 (2001) 5728–5737, https://doi.org/10.1021/bi010067e.
[86] P.L. Dutton, D.F. Wilson, Redox potentiometry in mitochondrial and photosynthetic bioenergetics, Biochim. Biophys. Acta. 346 (1974) 165–212, https://doi.org/10.1016/0304-4173(74)90008-1.
[87] C.H. Foyer, G. Noctor, Ascorbate and glutathione: the heart of the redox hub, Plant Physiol. 155 (2011) 2–18, https://doi.org/10.1104/pp.110.167569.
[88] A.G. Mauk, G.R. Moore, Control of metalloprotein redox potentials: what does site-directed mutagenesis of hemoproteins tell us? J. Biol. Inorg. Chem. 2 (1997) 119–125, https://doi.org/10.1007/s007750050115.
[89] K.K. Rodgers, S.G. Sligar, Surface electrostatics, reduction potentials, and the internal dielectric-constant of proteins, J. Am. Chem. Soc. 113 (1991) 9419–9421, https://doi.org/10.1021/ja00024a087.
[90] S.P. Rafferty, J.G. Guillemette, A.M. Berghuis, M. Smith, G.D. Brayer, A.G. Mauk, Mechanistic and structural contributions of critical surface and internal residues to cytochrome c electron transfer reactivity, Biochemistry. 35 (1996) 10784–10792, https://doi.org/10.1021/bi960430v.
[91] J.P. Bustamante, L. Radusky, L. Boechi, D.A. Estrin, A. ten Have, M.A. Martí, Evolutionary and functional relationships in the truncated hemoglobin family, PLoS Comput. Biol. 12 (2016) 26, https://doi.org/10.1371/journal.pcbi.1004701.
[92] M.H. Ahmed, M.S. Ghatge, M.K. Safo, Hemoglobin: structure, function and allostery, Subcell. Biochem. 94 (2020) 345–382, https://doi.org/10.1007/978-3-030-41769-7_14.
[93] W.R. Montfort, A. Weichsel, J.F. Andersen, Nitrophorins and related antihemostatic lipocalins from *Rhodnius prolixus* and other blood-sucking arthropods, Biochim. Biophys. Acta. 1482 (2000) 110–118, https://doi.org/10.1016/s0167-4838(00)00165-5.
[94] D.K. Menyhard, G.M. Keseru, Protonation state of Asp30 exerts crucial influence over surface loop rearrangements responsible for NO release in nitrophorin 4, FEBS Lett. 579 (2005) 5392–5398, https://doi.org/10.1016/j.febslet.2005.09.003.
[95] N.V. Di Russo, M.A. Martí, A.E. Roitberg, Underlying thermodynamics of pH-dependent allostery, J. Phys. Chem. B. 118 (2014) 12818–12826, https://doi.org/10.1021/jp507971v.
[96] F.J. Braun, P. Hegemann, Direct measurement of cytosolic calcium and pH in living *Chlamydomonas reinhardtii* cells, Eur. J. Cell Biol. 78 (1999) 199–208, https://doi.org/10.1016/S0171-9335(99)80099-5.
[97] W. Kabsch, C. Sander, Dictionary of protein secondary structure: pattern recognition of hydrogen-bonded and geometrical features, Biopolymers. 22 (1983) 2577–2637, https://doi.org/10.1002/bip.360221211.